Biomaterials 299 (2023) 122174

Contents lists available at ScienceDirect

Biomaterials

journal homepage: www.elsevier.com/locate/biomaterials

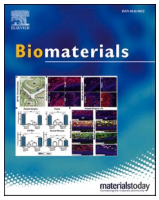

Heart-derived collagen promotes maturation of engineered heart tissue

Hidenori Tani [a,b], Eiji Kobayashi [c,e,**], Shinomi Yagi [f], Keisuke Tanaka [f], Kotaro Kameda-Haga [a], Shinsuke Shibata [d,g], Nobuko Moritoki [d], Kaworu Takatsuna [a], Taijun Moriwaki [a], Otoya Sekine [a], Tomohiko C Umei [a], Yuika Morita [a,h], Yusuke Soma [a], Yoshikazu Kishino [a], Hideaki Kanazawa [a], Jun Fujita [a,i], Shunji Hattori [e], Keiichi Fukuda [a], Shugo Tohyama [a,*]

[a] Department of Cardiology, Japan
[b] Joint Research Laboratory for Medical Innovation in Heart Disease, Japan
[c] Department of Organ Fabrication, Japan
[d] Electron Microscope Laboratory, Keio University School of Medicine, Shinjuku, Tokyo, Japan
[e] Department of Kidney Regenerative Medicine, The Jikei University School of Medicine, Tokyo, Japan
[f] Nippi Research Institute of Biomatrix, Toride, Ibaraki, Japan
[g] Division of Microscopic Anatomy, Graduate School of Medical and Dental Sciences, Niigata University, Niigata, Japan
[h] Kanagawa Institute of Industrial Science and Technology (KISTEC), Kawasaki, Kanagawa, Japan
[i] Department of Pathology & Immunology, Baylor College of Medicine, Houston, TX, USA

ARTICLE INFO

Keywords:
Human induced pluripotent stem cells
Tissue engineering
Engineered heart tissue
Extracellular matrix
Collagen

ABSTRACT

Although the extracellular matrix (ECM) plays essential roles in heart tissue engineering, the optimal ECM components for heart tissue organization have not previously been elucidated. Here, we focused on the main ECM component, fibrillar collagen, and analyzed the effects of collagens on heart tissue engineering, by comparing the use of porcine heart-derived collagen and other organ-derived collagens in generating engineered heart tissue (EHT). We demonstrate that heart-derived collagen induces better contraction and relaxation of human induced pluripotent stem cell-derived EHT (hiPSC-EHT) and that hiPSC-EHT with heart-derived collagen exhibit more mature profiles than those with collagens from other organs. Further, we found that collagen fibril formation and gel stiffness influence the contraction, relaxation, and maturation of hiPSC-EHT, suggesting the importance of collagen types III and type V, which are relatively abundant in the heart. Thus, we demonstrate the effectiveness of organ-specific collagens in tissue engineering and drug discovery.

1. Introduction

The combined use of cardiomyocytes (CMs) differentiated from human induced pluripotent stem cells (hiPSCs) and *in vitro* 3D heart tissue-construct engineering, which can induce structural and functional maturation better than 2D cultures, brings new perspectives for elucidating heart diseases, drug development, and tissue replacement therapy. Several studies have reported the spontaneous formation of 3D CM aggregates; furthermore, Eschenhagen et al. have established technologies to infer contractile forces in human induced pluripotent stem cell (hiPSC)-derived engineered heart tissue (hiPSC-EHT) [1–9].

The extracellular matrix (ECM) regulates cell behavior by modulating biochemical signals and the mechanical properties of the microenvironment, playing a significant role in 3D tissue engineering [10,11]. The most commonly used hydrogels in EHT are the natural ECM protein collagen type I and Matrigel (ECM from Engelbreth–Holm–Swarm tumors in mice, containing mainly laminin-111, nidogen, and collagen type IV) [1,2]. The blood-clotting material fibrin based, ring-type EHT with medical-grade bovine collagen without Matrigel, has been reported with a detailed description of the EHT matrix and serum components [12]. Supplementation with mesenchymal stem cells and fibroblasts has been shown to promote structural, mechanical, and molecular maturation of collagen type I and Matrigel-based EHT [13]. Decellularized ECM (dECM) provides an efficient bioscaffold with complex structural and biochemical cues; cardiac dECM therefore enhances EHT maturation by mimicking the native niche microenvironment for tissue maintenance [14–19]. Elasticity is an important factor in native niche-microenvironment mimicry. The relationship between ECM

* Corresponding author.
** Corresponding author. Department of Organ Fabrication, Japan.
E-mail addresses: eijikoba@jikei.ac.jp (E. Kobayashi), shugotohyama@keio.jp (S. Tohyama).

https://doi.org/10.1016/j.biomaterials.2023.122174
Received 31 August 2022; Received in revised form 17 May 2023; Accepted 19 May 2023
Available online 29 May 2023

elasticity and CM behavior has been investigated, revealing that *in vitro* mimicking in scaffolds of *in vivo* stiffness enhances CM differentiation, reprogramming, and maturation [20–25]. ECM elasticity affects the surface membrane integrin, thereby activating signaling pathways such as focal adhesion kinase (FAK), phosphoinositide 3-kinase (PI3K)/AKT, Jun amino terminal kinase (JNK), Rho-associated protein kinase (ROCK), and extracellular signal-regulated kinases (ERK) 1 and 2 [26,27]. ECM elasticity seems to also be related to myofibril organization and mitochondrial function, resulting in heart tissue maturation [28–30]. However, the optimal ECM components for 3D heart tissue constructs remain unknown.

Quantification of a decellularized human heart has revealed that the main constituents of the human heart are fibrillar collagen, particularly type I collagen [31]. Although the composition ratio and nature of collagen differ among organs and the components of ECMs change dynamically at each developmental stage, most commercially available collagen is either skin-derived, comprising predominantly type I collagen with type III at 15–25%, or purified type I collagen [32–36]. Intrinsically, the careful selection and control of ECM components and their composition must be of importance in tissue engineering. Nonetheless, most of the methods of heart tissue engineering do not take this into account, and use ECMs that are not derived from the heart. Moreover, the effects on tissue engineering of using collagen from different organs have not previously been elucidated.

To address this, we analyzed differences in the effects of using collagens from types of six porcine organs on hiPSC-EHT organization, and examined why heart-derived collagen is superior for generating hiPSC-EHT.

2. Materials and methods

2.1. Cell lines and culture

The cells were cultured in a humidified 5% CO_2 incubator at 37 °C and routinely tested for mycoplasma contamination. The hiPSC lines (201B7, 253G4) were provided by the Center for iPS Cell Research and Application, Kyoto University. They were maintained in mTeSR1 medium (Stemcell Technologies, Vancouver, Canada). The medium was passaged every 2 d and the cells were passaged every 7 d. Following passage, the cells were washed with D-PBS and incubated for 3 min with TrypLE Select (Thermo Fisher Scientific, 12563–011; Waltham, MA) at 37 °C. The cells were collected in a medium with 10 μM Y-27632 and pelleted for 4 min at 300 RCF. The cells were resuspended and counted using a Vi-CELL counter (Beckman Coulter, Brea, CA), then plated in dishes coated with Matrigel (BD Bioscience, 356230).

Porcine neonatal cardiac fibroblasts (CFs) were isolated using the outgrowth method from heart tissue blocks, and were maintained using FGM-3 BulletKit (Lonza, CC-4526; Basel, Switzerland). The medium was changed every 2-3 d and the cells were passaged every 7 d. Following passage, the cells were washed with the same medium and incubated for 5 min with Accutase at 37 °C. The cells were collected in the same medium and pelleted for 4 min at 300 RCF. The cells were resuspended and counted using a Vi-CELL counter. Finally, the cells were plated in fibronectin-coated dishes. Human neonatal ventricular CFs were purchased (Lonza, CC-2904) and maintained with FGM-3 BulletKit (Lonza, CC-4526). The cells were counted using Vi-CELL, then plated in fibronectin-coated dishes.

2.2. Cardiomyocyte differentiation from hiPSCs

hiPSCs were differentiated into CMs, as described previously [37–39]. Briefly, on day 0, the cells were rinsed with D-PBS and incubated for 1 day with RPMI-1640 (FUJIFILM Wako Pure Chemical Corporation, 189–02025; Tokyo, Japan) supplemented with a 2% B27 supplement (without insulin) (Thermo Fisher Scientific, A1895601) and 6 μM CHIR99021 (FUJIFILM Wako Pure Chemical, 034–23103). The next day (on day 1), the cells were rinsed with D-PBS and incubated with RPMI-1640 supplemented with B27 without insulin. On day 3, the cells were incubated with RPMI-1640 supplemented with B27 (without insulin) and 5 μM IWR-1 (Sigma-Aldrich, I0161-25 MG; St Louis, MO). On day 6, the cells were rinsed with D-PBS and incubated with RPMI-1640 supplemented with B27 without insulin. On day 7, the cells were incubated with MEM-α (Thermo Fisher Scientific, 12571–048) supplemented with 5% FBS (Biowest, S1560-500; Nuaillé, France) and 2 mM sodium pyruvate (Sigma-Aldrich, S8636-100 ML). On days 10–14, the cells were metabolically selected with StemFit AS501 medium (Ajinomoto, Tokyo, Japan) [38,40]. On days 14–16, the cells were incubated with MEM-α supplemented with 5% FBS and 2 mM sodium pyruvate.

2.3. Generation of hiPSC-derived engineered heart tissue (hiPSC-EHT)

Metabolically purified hiPSC-CMs (hiPSC-derived CMs) (day 15 or day 16 of the differentiation culture) were rinsed twice with D-PBS and incubated for 10 min with trypsin–EDTA solution (Nacalai Tescque, 35554–64; Kyoto, Japan) at 37 °C. Dissociated cells were pelleted for 4 min at 300 RCF. The cells were resuspended in MEM-α supplemented with 5% FBS and 2 mM sodium pyruvate and counted using a Vi-CELL counter.

We generated hiPSC-EHT in agarose casting molds with solid silicone racks (EHT Technologies, C0002 and C0001, respectively; Hamburg, Germany), as previously described [2,41,42]. In brief, casting molds were generated with agarose (2% in D-PBS) in 24-well plates (Corning, New York, NY). After solidification, the silicone racks were placed in the plates. The cells (95% CMs and 5% CFs, final concentration; 1×10^7 cells/mL) were mixed with 50 or 100 μL/mL Matrigel, 1 mg/mL each kind of collagen, 5 mg/mL bovine fibrinogen (200 mg/mL in NaCl 0.9% + 0.5 mg/mg aprotinin [Sigma-Aldrich, A1153]), and 2 × DMEM (matching the volume of fibrinogen and thrombin for isotonization). The Rho-kinase inhibitor Y-27632 (0.1%) was also added to prevent cell death during casting. For each EHT sample, 100 μL of the reconstitution mix with 3 μL thrombin was pipetted into the casting molds. After fibrin polymerization (37 °C, 2 h), the silicone racks with attached fibrin gels were transferred to new 24-well plates and cultured for up to 6 weeks (37 °C, 20% O_2, 5% CO_2). The culture medium consisted of MEM-α, supplemented with 5% FBS, 2 mM sodium pyruvate, and 33 mg/mL aprotinin, and was changed every 2 d. After approximately 1 week in culture, the hiPSC-EHT displayed spontaneous coherent, regular beating, deflecting the silicone posts.

2.4. Preparation of tissue-derived crude collagens

Adult (6 month-old) porcine hearts, spleens, kidneys, livers, lungs, and skin were purchased from Tokyo Shibaura Zoki. These organs were minced and washed several times with a 10% NaCl solution. The washed organs were homogenized in fresh 10% NaCl solution and centrifuged at 10,000 RCF for 30 min at 4 °C. The pellet was washed several times with the same solution, suspended in ethanol to remove lipids, and filtered using filter paper. The collagen was extracted from the final pellet by gentle shaking at 4 °C in 50 mM acetic acid containing 5 mg/mL pepsin (Sigma-Aldrich). After centrifugation, 4 M NaCl in 50 mM acetic acid was added to the supernatant at the final concentration of 2 M NaCl to precipitate collagens. After centrifugation, distilled water was added to the pellet, and the collagen was completely solubilized. Phosphate buffer (pH 8.0) was then added to neutralize it to a final concentration of 10 mM phosphate. The mixture was incubated overnight at 25 °C and then centrifuged to precipitate collagen. The precipitates were dissolved in 5 mM acetic acid and the collagen concentration was adjusted to 5 mg/mL.

2.5. Contractile analysis of hiPSC-EHT

Contractile analysis was performed using an SI8000 live-cell motion

imaging system (Sony Corporation, Tokyo, Japan). The contraction peaks were analyzed in terms of the beating rate, force, contraction duration (CD), and relaxation duration (RD). Deformation velocity, obtained using the SI8000 imaging system, was transformed into deformation distance using Python, and RD_{80}, CD_{80}, RD_{50}, and CD_{50} were calculated (Fig. S7C).

2.6. Flow cytometry (FACS)

To detect cTnT expression using flow cytometry (FACS), the cells were dissociated using 0.25% trypsin–EDTA and then fixed with 4% PFA for 20 min. Subsequently, the cells were permeabilized with 0.1% Triton X-100 (Sigma-Aldrich) at room temperature for 5 min, incubated with cTnT antibody (Thermo Fisher Scientific, MS-295-P1) at 4 °C overnight, and incubated with the Alexa 488 donkey anti-mouse immunoglobulin G (IgG) secondary antibody (Life Technologies, Carlsbad, CA) at room temperature for 2 h. To compare tetramethylrhodamine methyl ester (TMRM) fluorescence intensity, the cells were dissociated using a gentleMACS dissociator (Miltenyi Biotec; Bergisch Gladbach, Germany) and C Tubes (Miltenyi Biotec). Briefly, after 4-week incubation, gently removed EHTs (more than eight EHTs per condition) were placed in a C tube filled with 1.5 mL Multi Tissue Dissociation solution kit 3 (Miltenyi Biotec), and the gentleMACS protocol (i. spin 0 15 min, ii. spin 300 30 s, iii. spin 0 7 min, iv. spin 20 8 min, v. spin 300 30 s) was performed. Dissociated cells were then incubated with 10 nM TMRM for 20 min. The cells were analyzed using a Gallios FACS instrument (Beckman Coulter).

2.7. Analysis of types I, III, and V collagen composition

Crude collagen was resolved using SDS-PAGE buffer (62.5 mM Tris–HCl, pH 6.8, 2% SDS, 10% glycerol, 5% 2-mercaptoethanol, and 0.02% bromophenol blue) and heated at 100 °C for 3 min. SDS-PAGE (5% gels containing 6 M urea) was performed under reducing conditions, and the gel was stained with Coomassie Brilliant Blue R-250. The band intensities of type I, III, and V collagen α-chains were quantified using ImageJ, and the composition of these collagens was calculated from the quantitative values. We evaluated collagen derived from each organ type (heart, spleen, kidney, liver, lung, and skin), and collagen derived from each site in the heart (left atrium, left ventricle, right atrium, right ventricle, epicardium, coronary artery, atrioventricular valve, semilunar valve).

2.8. Fibril formation assay

The collagen sample (0.5 mg/mL) in PBS (pH 7.4) was placed in a 96-well plate (Corning) (300 μL/well), and turbidity was monitored at 37 °C and 520 nm using an SH-9000 microplate reader (Corona Electric, Ibaraki, Japan).

2.9. Measurement of gel stiffness

Four volumes of collagen stock solution (2.5 mg/mL) were mixed with 2.5 × DMEM (4 vol), 2.5% $NaHCO_3$ (1 vol), and PBS (−) (1 vol) to prepare a 1 mg/mL collagen solution. The mixture was incubated in a 48-well plate (1 mL gel/well) at 37 °C for 20 h to allow gelation. The physical properties of the collagen gels were measured using a creep meter (Rheoner RE-33005; Yamaden Co. Ltd., Tokyo, Japan). A gel sample in a 48-well plate was pressed using a flat plunger (3 mm diameter) at 0.5 mm/s. The loading stress of the plunger due to the deformation of the sample gel was monitored, and the gel stiffness was defined as the breaking stress; the slope of the stress-strain curve decreased at a strain of 10%.

2.10. Atomic force microscopy (AFM)

AFM was performed using an SPM-9500 J2 scanning probe microscope (Shimadzu, Kyoto, Japan) equipped with a piezoelectric scanner; the maximum widths in the x, y, and z scan ranges were 125, 125, and 8 μm, respectively. A cantilever with a silicon tip was used at a force constant of 42 N/m and resonance frequency of 320 kHz (NCHR-20; NanoWorld, Neuchâtel, Switzerland). Height and phase images were obtained simultaneously in dynamic mode in air. The scan speed was maintained at 1 Hz. The collagen sample (0.2 mg/mL) in PBS (pH 7.4) was placed on a cover glass and incubated at 37 °C for 5 h. The samples were then fixed with 4% paraformaldehyde (PFA). After extensive washing with distilled water, the fixed collagen fibers were air-dried and processed for AFM analysis. The thickness of the collagen fibers was measured using ImageJ analysis of the obtained AFM images.

2.11. Purification of types I, III, and V collagen

Salt precipitation was performed to fractionate the various collagen types present in the crude collagen solution. Briefly, the crude acidic collagen solution was adjusted to neutral pH, and the NaCl concentration was set to 1.6 M to precipitate type III collagen and fractionate types I and V collagen. Precipitated type III collagen was resuspended in 5 mM acetic acid. The supernatant containing types I and V collagen was adjusted to 0.7 M NaCl at acidic pH to precipitate type I collagen. After centrifugation, type V collagen in the supernatant was precipitated by adding solid NaCl to 2 M. Each pellet was dissolved in 5 mM acetic acid. The solubilized collagen was dialyzed against 5 mM acetic acid and used for further experiments.

2.12. Quantification of collagen content via liquid chromatography–mass spectrometry (LC-MS)

The collagen content of the hiPSC-EHT was evaluated based on the amount of hydroxyproline, as previously described [45]. Briefly, freeze-dried hiPSC-EHT samples were hydrolyzed by heating at 110 °C with 6 M HCl for 20 h. The acid-hydrolyzed samples were dried using a centrifugal evaporator CVE-3100 (Eyela, Tokyo, Japan) after adding the acid hydrolysate of stable isotope-labeled collagen (SI-collagen) as an internal standard [46,47]. The samples were dissolved in 0.1% acetic acid/5 mM ammonium acetate in 50% acetonitrile and analyzed via LC-MS in multiple reaction monitoring (MRM) mode on a QTRAP 5500+ hybrid triple quadrupole/linear ion trap mass spectrometer (AB Sciex, Foster City, CA) coupled to an ExionLC AD HPLC system (AB Sciex) using a ZIC-HILIC column (3.5 μm particle size, L × I.D. 150 mm × 2.1 mm) (Merck Millipore, Billerica, MA). The collagen content was determined using the peak area ratio of hydroxyproline relative to $^{13}C_5^{15}N_1$-hydroxyproline derived from SI-collagen.

The amounts of types I and III collagen were determined via LC-MS analysis of tryptic marker peptides, as previously reported [46,48]. Briefly, freeze-dried hiPSC-EHT samples were heated at 60 °C for 30 min in 100 mM Tris–HCl/1 mM $CaCl_2$ (pH 7.6) after adding SI-collagen as an internal standard. The samples were digested using sequencing-grade modified trypsin (Promega) at 37 °C for 16 h. Trypsin digestion was again performed at 37 °C for 24 h after heating at 60 °C for 30 min. After centrifugation, the supernatant was subjected to LC-MS analysis with chromatographic separation using a BIOshell A160 peptide C18 HPLC column (5 μm particle size, L × I.D. 150 mm × 2.1 mm; Supelco, Bellefonte, PA). Tryptic marker peptides for α1(I), α2(I), and α1(III) chains were newly selected to be specific to human sequences (differing from porcine sequences) or common to human and porcine sequences (Table S1), and were detected in MRM mode. The amounts of types I and III collagen were determined using the peak area ratio of the marker peptides relative to the corresponding stable SH-9000 microplate reader (Corona Electric, Ibaraki, Japan) isotope-labeled (heavy) peptides derived from SI-collagen.

2.13. qRT-PCR

The samples were disrupted and homogenized in TRIzol (Invitrogen, Waltham, MA) using a TissueLyser LT (Qiagen, Hilden, German) instrument. Total RNA was extracted using the ReliaPrep RNA Cell Miniprep System (Promega, Z6012; Madison, WI), according to the manufacturer's protocol. One sample was extracted from at least four hiPSC-EHT samples generated under the same conditions. mRNA (1 μg) was reverse-transcribed into cDNA using Oligo (dT) with SuperScript II Reverse Transcriptase (Invitrogen). qRT-PCR was performed using the StepOnePlus Real-Time PCR system with TaqMan probes (Applied Biosystems, Waltham, MA) (Table S2). Expression was normalized against that of the housekeeping gene glyceraldehyde 3-phosphate dehydrogenase (GAPDH).

2.14. Gene microarray analyses

Total RNA was extracted from hiPSC-EHT as described. Extracted RNA was quantified using an Agilent Low Input Quick Amp Labeling Kit (Agilent Technologies, Santa Clara, CA). Gene expression was determined via microarray analysis according to the manufacturer's instructions. The raw data for each spot were normalized via substitution, with the mean intensity of the background signal determined using the combined signal intensities of all blank spots with 95% confidence intervals. The signals detected for each gene were normalized using the global normalization method. The cut-off value of absolute fold change >1.5 was used to select for genes that were differentially expressed between the sample groups. Volcano plots were generated using the moderated *t*-test using GeneSpring v. 12.6 (Agilent). Gene set enrichment analysis (GSEA) was performed using GSEA v. 4.0.1 to test specific gene sets, as previously described [43]. Gene ontology (GO) enrichment analysis for the 'biological function' category was performed using DAVID v. 6.8, a gene functional annotation and classification tool [44]. GO groups were selected for significance using a p-value cut-off of 0.05. The sample of fetal heart was purchased (Clontech Laboratories, 636583; Mountain View, CA).

2.15. Western blotting

After dissociation in gentleMACS M Tubes (Miltenyi Biotec) filled with 1 mL M-PER Mammalian Protein Extraction Reagent using the gentleMACS Program Protein_01, the lysates were collected and lysed with M-PER Mammalian Protein Extraction Reagent plus phosphatase and protease inhibitors (Thermo Fisher Scientific). After sonication using an ultrasonic disruptor (TOMY, UR–21 P; Tokyo, Japan), insoluble cell debris was pelleted (at 14,000 rcf for 20 min) and the resulting supernatant was used for analysis. Thereafter, 100 μg of protein was loaded into each well of a NuPAGE 4–12% Bis-Tris gel (Thermo Fisher Scientific, NP0321BOX). Subsequently, electrophoresis was performed at 200 V for 35 min in NuPAGE MES SDS running buffer (Thermo Fisher Scientific, NP0002). Transfer was performed using iBlot2 PVDF mini Stacks (Thermo Fisher Scientific, IB24002) and an iBlotTM 2 Gel Transfer Device (Thermo Fisher Scientific, IB21001) according to the manufacturer's instructions. Following transfer, membranes were blocked with Blocking One (Nacalai Tesque, 03953) for 30 min and rinsed with ultrapure water. Membranes were probed with primary antibodies against GAPDH (1:25000, mAB#4695; Cell Signaling, Danvers, MA), MYL2 (1:1000, ab79935; Abcam, Cambridge, UK), MYL7 (1:1000, 311011; Synaptic Systems, Göttingen, Germany), TNNI1 (1:2000, NBP2-46170; Novus Biologicals, Centennial, CO), TNNI3 (1:10000, ab52862; Abcam), CX43 (1:5000, ab117843; Abcam), and CASQ2 (1:1000, ab108289; Abcam) diluted in TBS-T overnight at 4 °C. Membranes were washed three times with TBS-T for 5 min each time, then probed with secondary anti-rabbit or anti-mouse IgG antibodies. After proteins were imaged using ChemiLumi One (Nacalai Tesque, 07880–70), the membranes were imaged using an iBright FL1000 imaging system (Thermo Fisher Scientific) and quantified using ImageJ (National Institutes of Health).

2.16. Histology

For immunocytochemistry, the hiPSC-EHT was carefully removed from the pillars, fixed in 4% PFA overnight, and embedded in O.C.T compound (Sakura Finetek, the Netherlands) for freezing in liquid nitrogen. Frozen hiPSC-EHT was cut into 10 μm sections to show the long-axis direction. Sections were stained with primary antibodies against cTnT (Thermo Fisher Scientific, MS-295-P1), fibronectin (Sigma-Aldrich, F3648), and connexin43 (Sigma-Aldrich, C6219), followed by incubation with secondary antibodies conjugated with Alexa 488 and 546 donkey anti-mouse immunoglobulin G (IgG) secondary antibody (Life Technologies). Images were acquired using a BZ-X710 microscope (Keyence, Osaka, Japan).

2.17. Transmission electron microscopy (TEM)

The samples were fixed in 2.5% glutaraldehyde in HEPES buffer, rinsed, and post-fixed in 1% OsO_4, then dehydrated in a series of increasing concentrations of ethanol, in acetone, in n-butyl glycidyl ether (QY1), and finally in a series of increasing concentrations of epoxy resin with QY1. The samples were then incubated in 100% epoxy resin (100 g epoxy resin contains 27.0 g MNA, 51.3 g EPOK-812, 21.9 g DDSA, and 1.1 mL DMP-30) at 4 °C to enhance infiltration. Specimens were polymerized in 100% epoxy resin at 60 °C for 72 h. From the area of interest, identified using semi-thin sectioning, ultrathin sections were prepared using a Leica UC7 ultramicrotome (Leica Microsystems, Tokyo, Japan). Ultrathin sections were examined via TEM (JEM1400 plus; Jeol, Tokyo, Japan).

2.18. Seahorse analysis

After 4-week incubation, gently removed EHTs were dissociated in gentleMACS C Tubes with gentleMACS dissociator as described in Section 2.6. Then, the dissociated cells were seeded on XF24 plates (Agilent, 103518–100; Santa Clara, CA) with 0.5 μg/cm^2 iMatrix-221 (Nippi, Tokyo, Japan) at a density of 1.0×10^5 cells per well. Mitochondrial respiration was measured using an XF24 Extracellular Flux Analyzer (Seahorse Bioscience, Agilent). One hour before measurement, the cells were incubated with Seahorse XF DMEM Medium (Agilent, 103575–100). The oxygen consumption rate (OCR) was determined using an XF Cell Mito Stress Test Kit (Agilent, 103015–100) with subsequent additions of (1) 1 μM oligomycin, (2) 1.5 μM carbonyl cyanide 4-(trifluoromethoxy) phenylhydrazone (FCCP), and (3) 0.5 μM rotenone/antimycin A. The OCR values were normalized to cell numbers per well. Baseline respiration was calculated by subtracting OCR, after the addition of rotenone and antimycin A, from the respiration at the first time point. Maximal OCR was calculated as the difference between OCR after FCCP infusion and OCR after rotenone and antimycin A infusion. Respiratory capacity was calculated by subtracting the difference between the OCR before the addition of oligomycin and after rotenone and antimycin A infusion from the OCR after FCCP infusion. ATP production was calculated as the OCR at the first time point minus the OCR after oligomycin infusion. The proton leak was determined by subtracting the OCR after FCCP infusion from the value after oligomycin infusion. Coupling efficiency was calculated as the proportion of the oxygen consumed to drive ATP synthesis compared with that driving proton leak and the fraction of basal mitochondrial OCR used for ATP synthesis (ATP-linked OCR/basal OCR).

2.19. Calcium transients

To determine intracellular calcium transients, the gently removed EHT was dissociated using the gentleMACS dissociator, then seeded on a

glass-bottom 24-well plate (MatTek Corporation, Ashland, MA) coated with 0.5 μg/cm^2 iMatrix-221 (Nippi) at a density of 2.0 × 10^5 cells per well. Following 2–3 d incubation, cells were loaded with Cal-520, AM (AAT Bioquest, Pleasanton, CA) for 90 min and analyzed with a BZ-X710 microscope and BZ-X800 Analyzer (Keyence) 30 min after room temperature incubation. The time to 50% decay was calculated from the decreasing limbs of the transients. Data were collected from 5 fields of view in each condition (n = 3).

2.20. Statistical analysis

The statistical parameters, including numbers of samples (at least n = 4), descriptive statistics, and significance, are described in the figures and figure legends. Each experiment was performed at least three times for each time point. Differences between groups were evaluated for statistical significance with Student's *t*-test. Log-rank tests were performed for Kaplan–Meier survival curves. Differences were regarded as

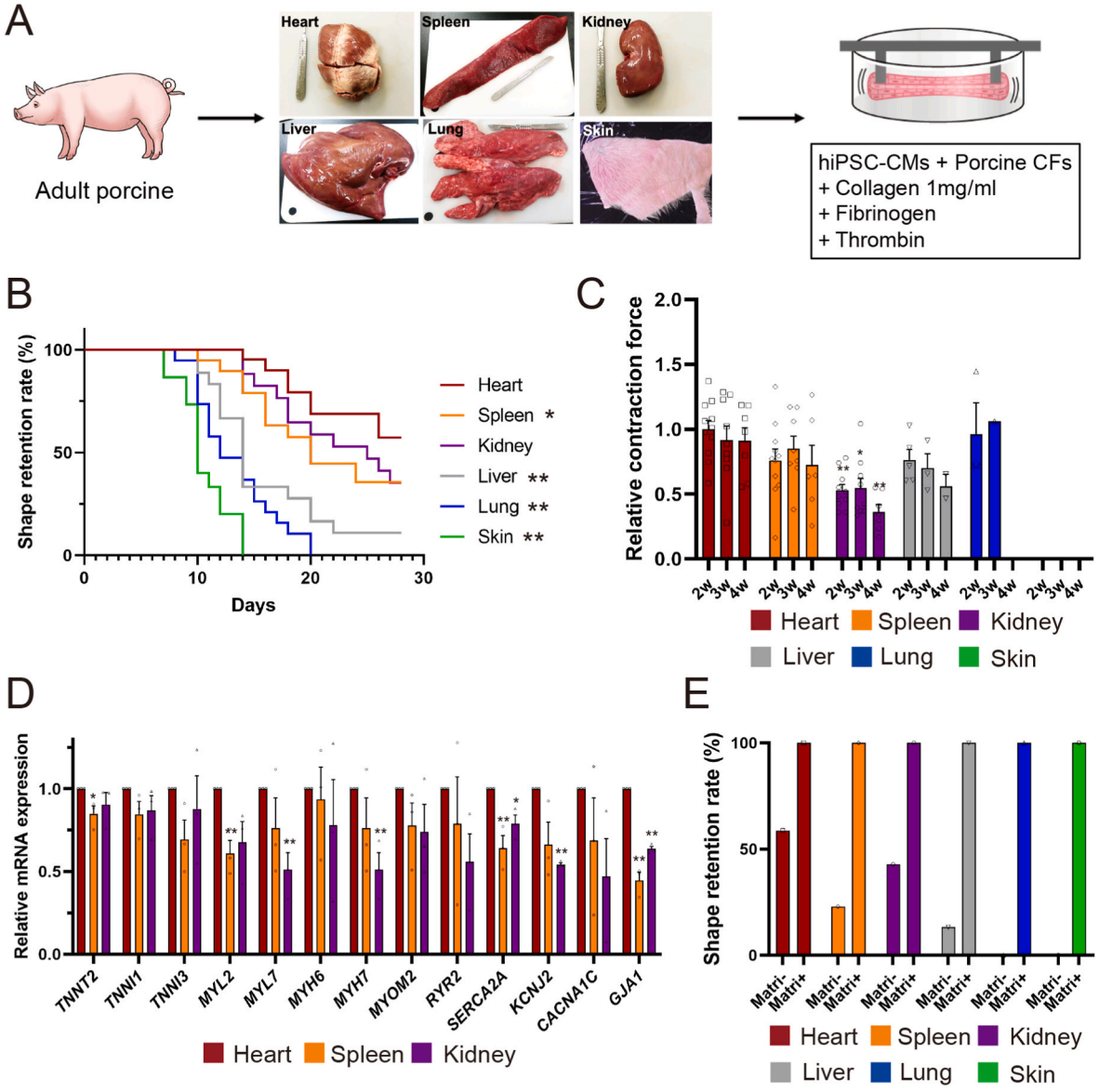

Fig. 1. Heart-derived collagen induces better contraction retention of human induced pluripotent stem cell-derived (hiPSC) engineered heart tissue (EHT)
(A) Schematic representation of collagen extraction from six types of porcine organs and of hiPSC-EHT generation. CM: cardiomyocyte; CF: cardiac fibroblast.
(B) Serial shape-retention rate of hiPSC-EHT generated using six different collagens (heart, spleen, kidney, liver, lung, and skin) (each n ≧ 16/4). The p-values were calculated for differences between hiPSC-EHT generated from heart-derived collagen or other organs-derived collagens.
(C) Relative contractile force of hiPSC-EHT generated using six different collagens at 2 weeks, 3 weeks, and 4 weeks (each n = 12/3). Contractile forces for hiPSC-EHT samples detached or deviated from the silicon rack pillars were not included. The average contractile force at 2 weeks of heart-derived collagen (Hc)-EHT was defined as the control value. Differences between hiPSC-EHT generated from heart collagen and other organs-derived collagens were regarded as significant at $p < 0.05$.
(D) qRT-PCR showing enrichment at 4 weeks of cardiac muscle- and ion-related genes in hiPSC-EHT generated using heart, spleen, and kidney collagen (n = 3). mRNA expression of EHT generated using heart collagen was defined as the control value. Differences between hiPSC-EHT generated using heart-derived collagen and using other organs-derived collagens were regarded as significant at $p < 0.05$.
(E) Shape retention rate at 4 weeks of hiPSC-EHT generated using six different collagens with or without Matrigel (each n ≧ 12/3
Replicates are indicated as EHT samples/number of independent experiments.
All data are presented as mean ± SEM; $*p < 0.05$, $**p < 0.01$. (For interpretation of the references to colour in this figure legend, the reader is referred to the Web version of this article.)

significant at $p < 0.05$. Statistical analyses were performed using GraphPad Prism v. 7.0 (GraphPad Software, San Diego, CA).

3. Results

3.1. Heart-derived collagen induces better contraction retention of hiPSC-EHT

Previous studies on hiPSC-EHT have mainly utilized skin-derived or purified type I collagen, Matrigel, and fibrin as scaffolds. Although decellularized ECM induces EHT maturation, the factors that induce this process remain to be elucidated. We generated and compared hiPSC-EHT with collagen derived from six types of porcine organs (the heart, spleen, kidney, liver, lung, and skin) to address this. First, we prepared crude collagen solution from adult porcine heart, spleen, kidney, liver, lung, and skin at 5 mg/mL. We then generated hiPSC-EHT by mixing metabolically purified hiPSC-CMs (cardiac Troponin T [cTnT] 99.47 ± 0.19%; Fig. S1A), porcine CFs, and each collagen at a final 1 mg/mL concentration (Fig. 1A). The shape retention rate (the probability of maintaining hiPSC-EHT autonomic contraction without the tissue becoming detached or deviating from the silicon rack pillars) depended on the organ of origin, with heart-derived collagen being superior (Fig. 1B and S1B). Most of the hiPSC-EHT generated using skin-derived collagen (Sc-EHT) became detached or deviated from the pillars within 2 weeks following organization (Fig. S1C), whereas half of that derived using heart-derived collagen (Hc-EHT) retained its shape and contraction after 1 month.

Next, the contractile force was calculated by measuring the distance between tissue-attachment points. At 2, 3, and 4 weeks after organization, Hc-EHT showed stronger contractile forces than those derived from other collagens, although without significant differences (Fig. 1C and S2A). hiPSC-EHT generated using lung-derived collagen showed seemingly higher contractile forces, and was almost entirely detached at 3 weeks. Since hiPSC-EHT generated using liver-, lung-, or skin-derived collagen could not retain its shape at 4 weeks, we analyzed the mRNA expression of hiPSC-EHT obtained using heart-, spleen-, or kidney-derived collagen. These hiPSC-EHT types comparatively retained their shape, and Hc-EHT exhibited the highest expression of various genes associated with CMs and ion channels (Fig. 1D).

We next examined the components of hiPSC-EHT, because an unstable tissue shape could substantially affect our findings. We attempted to substitute heart collagen with conventional components, finding that hiPSC-EHT generated without fibrinogen could not initially set into gelatin-like states; EHT generated using half as much fibrinogen could not retain its shape for 4 weeks; and EHT generated without thrombin or Matrigel could not retain stable contraction (Table 1). Grounded on the collagen-based organization method, a relatively stronger force with stable shape retention at 4 weeks was obtained by mixing heart collagen at a final 1 mg/mL concentration with fibrinogen, thrombin, and half as much Matrigel as is conventionally used [41]. Moreover, although we also tried to substitute laminin 221 and laminin 511 E8 fragment (iMatrix-221 and iMatrix-511) for Matrigel, the contractile force at 2 weeks of hiPSC-EHT generated using these substitutes was weaker than that obtained using Matrigel, and they could not retain their shape for 4 weeks (Fig. S2B). We achieved stable shape retention for 4 weeks after organization only by using Matrigel at half the amount of the conventional method, along with collagen from each organ (Fig. 1E).

3.2. Differences between collagens in terms of fibril formation and gel stiffness cause differences in hiPSC-EHT

Next, we attempted to identify what induced the differences in the shape retention rate of hiPSC-EHT induced with each collagen. Using a creep meter, we compared the physical properties of gels prepared with collagen derived from each organ type. Those prepared with heart-, spleen-, and liver-derived collagens were the stiffest, followed by those prepared with lung-, skin-, and kidney-derived collagens (Fig. S3A). This trend is similar to the differences in shape retention rate using collagens from different organs (Fig. 1B). Next, a turbidity assay was conducted on the reconstituted collagen fibrils. In this assay, changes in turbidity over time reflect the state of the reconstituted fibrils. For example, two factors influence changes in turbidity: 1) the number of covalently and non-covalently associated collagen molecular polymers initially present in the collagen solution, and 2) the ratio of types I, III, and V collagen in the solution. Fibrils containing more type III and V collagen are smaller in diameter. For the same collagen concentration, turbidity is lower when there are thinner fibrils (Fig. S3B). The turbidity of the skin-derived collagen samples was higher than that of the collagen from other origins, while the collagen samples derived from the heart, spleen, and kidney had lower turbidity. This suggests that reconstituted collagen fibrils from the heart, spleen, and kidney were thinner than those from the skin (Fig. 2A). Atomic force microscopy (AFM) observations revealed that the heart, spleen, and kidney collagen produced thinner reconstituted fibrils than the other organs (Fig. 2B and S3C).

To identify what induces these differences in collagen fibrils, we used SDS-PAGE analysis to quantify the composition of the major fibrillar collagens, types I, III, and V. Collagen from the heart contained a higher percentage of types III and V than other organs (Fig. 2C and S3D). The composition of types I, III, and V varied greatly depending on the region of the heart, with the left ventricle, which contracts most dynamically,

Table 1
Optimization of components of EHTs.

Heart collagen	Fibrinogen	Matrigel	Thrombin	Organization rate at 0 week	Shape retention rate at 2 weeks	Relative force at 2weeks	Shape retention rate at 4 weeks	Relative force at 4 weeks	Note
–	+	+	+	12/12 (100%)	12/12 (100%)	1.00	12/12 (100%)	1.04	conventional method
++	+	+	+	12/12 (100%)	12/12 (100%)	0.58	10/12 (83%)	1.06	
+	+	+	+	12/12 (100%)	12/12 (100%)	0.72	12/12 (100%)	0.99	
±	+	+	+	12/12 (100%)	12/12 (100%)	0.79	12/12 (100%)	1.14	
+	+	±	+	12/12 (100%)	12/12 (100%)	1.06	12/12 (100%)	1.24	best method
+	+	–	+	12/12 (100%)	11/12 (92%)	0.86	7/12 (58%)	1.48	unstable
+	±	+	+	12/12 (100%)	6/12 (50%)	1.12	0/12 (0%)	–	
+	±	–	+	12/12 (100%)	3/12 (25%)	1.13	0/12 (0%)	–	
+	–	+	+	0/12 (0%)	0/12 (0%)	–	0/12 (0%)	–	
+	–	–	+	0/12 (0%)	0/12 (0%)	–	0/12 (0%)	–	
+	+	+	–	12/12 (100%)	12/12 (100%)	0.71	6/12 (50%)	1.00	lean, unstable
+	–	+	–	0/12 (0%)	0/12 (0%)	–	0/12 (0%)	–	
+	+	–	–	12/12 (100%)	9/12 (75%)	0.52	3/12 (25%)	1.48	lean, unstable

+, base amount; ++, double amount; ±, half amount; −, not present.
Base amounts: Heart collagen, 1 mg/mL; Fibrinogen, 5 mg/mL; Matrigel, 100 μL/mL.
Relative forces are normalized to the force obtained using the conventional method at 2 weeks.

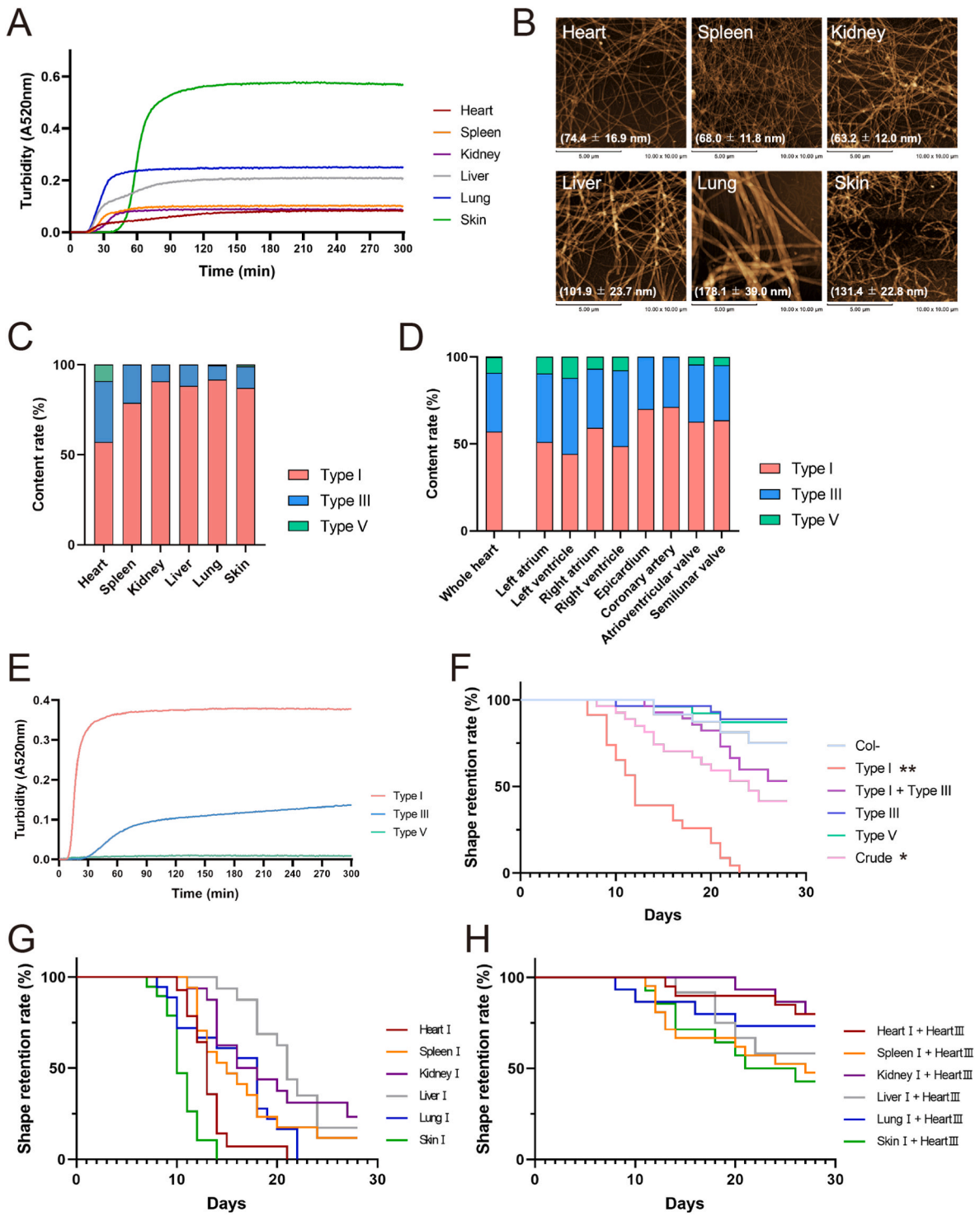

Fig. 2. Differences between collagens in fibril formation and gel stiffness cause differences in human induced pluripotent stem cell-derived (hiPSC) engineered heart tissue (EHT)

(A) Collagen turbidity, reflecting the fibrillogenesis of the collagen from each organ type, measured at 37 °C and 520 nm

(B) Atomic force microscopy (AFM) imaging of the fibrils of each collagen type. Scale bars indicate 5 μm

(C) Fibrillar collagen content in the collagen from each organ type

(D) Fibrillar collagen content in the various heart sites

(E) Turbidity for each type of heart collagen, reflecting fibrillogenesis, measured at 37 °C and 520 nm

(F) Serial shape retention rate of hiPSC-EHT generated using each type of fibrillar collagen (each n ≧ 24/4). The p-values were calculated for differences between hiPSC-EHT generated without collagen and with each type of fibrillar collagen

(G) Serial shape retention rate of hiPSC-EHT generated using type I collagen from each type of organ (each n ≧ 16/4). (H) Serial shape retention rate of hiPSC-EHT generated using type I collagen from each type of organ, and type III collagen from the heart (each n ≧ 16/4)

Replicates are indicated as EHT samples/number of independent experiments.

containing the greatest amounts of types III and V (Fig. 2D and S3E). These results indicate that type III and V collagens may play important roles in maintaining intense contractions in muscle tissue.

Next, we purified types I, III, and V collagen from crude heart collagen, and analyzed reconstituted fibril formation via a turbidity assay. Types III and V formed thinner fibrils than type I, with type V forming the thinnest fibrils (Fig. 2E). We generated hiPSC-EHT using heart-derived type I and III collagens, crude collagen, and in the absence of collagen, by mixing metabolically purified hiPSC-CMs, porcine CFs, and each collagen at a final 1 mg/mL concentration, without Matrigel. Although type III and V collagens were not completely purified (purity of type III: 88.2%; purity of type V: 97.2%), we confirmed that hiPSC-EHT generated using abundant type III collagen retained its shape significantly better than hiPSC-EHT generated using purified type I collagen (Fig. 2F and S4). Notably, hiPSC-EHT generated using purified type I collagens from each of the six organ types showed lower shape retention tendency than those generated using crude collagen from each type of organ, except for the samples generated from lung and liver collagen (Figs. 1B and 2G). These low shape retention rates were significantly improved by adding 40% heart-derived type III collagen (Fig. 2H). These results suggested that type III collagen, abundant in the heart and particularly in the left ventricle, plays an important role in maintaining hiPSC-EHT structure that can maintain pulsation and retain tissue shape.

3.3. Heart-derived collagen promotes cardiac maturation of hiPSC-EHT

Skin-derived collagen showed the most distant tendency from heart-derived collagen in terms of collagen fibril profiles and has been the most commercially common collagen. Therefore, to determine the molecular profile induced by organization using heart-derived collagen, we compared Hc-EHT with Sc-EHT and hiPSC-EHT without collagen as the control. We generated hiPSC-EHT by mixing metabolically purified hiPSC-CMs, porcine CFs, Matrigel, and each collagen at a final 1 mg/mL concentration. We compared the expression level of genes encoding sarcomeric proteins (*TNNT2, TNNI1, TNNI3, MYL2, MYL7, MYH6, MYH7*, and *MYOM2*, which has been known as an independent CM maturation marker), calcium-handling proteins (*RYR2, SERCA2A, CACNA1C*), and genes associated with electrophysiological development (*GJA1, KCNJ2*) using qRT-PCR at 4 weeks after organization, which revealed the upregulation of some maturation-related genes in Hc-EHT relative to Sc-EHT and hiPSC-EHT without collagens (Fig. 3A) [49].

To elucidate how the different collagens might impact cardiomyocyte maturation and overall function, we performed bulk transcriptomic analysis of hiPSC-EHTs generated with skin- and heart-derived collagens three weeks post-EHT formation. Differential gene expression analyses demonstrated that 2220 genes were upregulated, while 1371 genes were downregulated >1.5 times in Hc-EHT relative to Sc-EHT (Fig. 3B). To identify the biological functions of these 2220 genes, we first performed GO analysis. The GO biological process classification indicated that heart-derived collagen activated signaling pathways such as G-protein coupled receptor signaling, cell surface receptor signaling, intracellular signaling, integrin-mediated signaling, and mechanical stimulation, and promoted Na, K, and Ca ion transport (Fig. 3C). Consistent with this, GSEA revealed that genes upregulated in Hc-EHT were enriched in clusters related to CMs, conduction, metabolism, ECM, proliferation, and development (Table 2). These results suggest that Hc-EHT has mature profiles, with shifts in numerous pathways and aspects of functional development (Fig. 3C). Sarcomeric genes such as *MYOM2*, ion channel-related genes such as *KCNJ2*, metabolism-related genes such as *ATP2A2*, and calcium handling-related genes such as *CASQ2* were upregulated in Hc-EHT compared with that in Sc-EHT, and most of these genes were upregulated at 6 weeks relative to 3 weeks (Fig. 3D, upper panel). This maturity was not as fully developed as that of the fetal heart. Most of the significantly upregulated genes in Hc-EHT relative to Sc-EHT were also upregulated in the fetal heart (Fig. 3D, lower panel).

We next analyzed the protein expression of some maturation-related genes and confirmed that TNNI3/TNNI1 and MYL2/MYL7 ratios were significantly upregulated in Hc-EHT relative to Sc-EHT and hiPSC-EHT without collagen (Fig. 4A). Although immunostaining for cTnT and fibronectin suggested that the CMs and fibrillar matrix align similarly in hiPSC-EHT with or without heart- or skin-derived collagen, high-power field immunostaining for cTnT and connexin-43 (GJA1) revealed that Hc-EHT had longer sarcomere lengths and higher expression of connexin-43 than Sc-EHT and hiPSC-EHT without collagen (Fig. 4B, S5A, and S5B). TEM analysis revealed that Hc-EHT CMs showed more mature trends with organized structures, including detectable Z lines, I bands, A bands, and H bands, than those of EHT without collagen; whereas Sc-EHT CMs showed less visible bands compared with Hc-EHT CMs (Fig. 4C).

Since GSEA revealed that genes upregulated in Hc-EHT were enriched in clusters related to mitochondrial function, we analyzed the oxygen consumption rate (OCR) of dissociated cells from hiPSC-EHT generated with or without heart- or skin-derived collagens, via Seahorse metabolic analysis. Hc-EHT CMs showed the highest OCR, followed by those from Sc-EHT and then hiPSC-EHT without collagens, indicating higher use of oxidative phosphorylation (Fig. 5A and B, and S6A). Basal and maximal respirations, spare respiratory capacity, and ATP production were higher in Hc-EHT CMs than in Sc-EHT and hiPSC-EHT without collagens; however, proton leak and coupling efficiency did not significantly alter (Fig. 5B and S6A). Via FACS, we compared the fluorescence intensity of TMRM, an indicator of intact mitochondrial membrane potential. Relative TMRM fluorescence was highest in Hc-EHT CMs (Fig. S6B). These results demonstrate metabolic maturation induced by using heart-derived collagen.

Taken together, these results suggest that Hc-EHT has both functional and structural mature profiles compared with Sc-EHT and hiPSC-EHT without collagens.

3.4. Heart collagen induces a more mature contraction–relaxation status in hiPSC-EHT by providing abundant type III collagen along with type V collagen

We next compared the contractile difference in collagen type by analyzing the contraction of hiPSC-EHT generated using heart-derived type I, III, and V collagen, crude collagen, or without collagen. We generated hiPSC-EHT using each collagen type and Matrigel. We first calculated the hiPSC-EHT widths two weeks after generating the hiPSC-EHT, demonstrating that hiPSC-EHT derived using heart-derived type I collagen were thinner, whereas hiPSC-EHT using heart-derived type III collagen were thicker (Fig. 6A and S7A). Consistent with this, hiPSC-EHT obtained using heart-derived type I collagen showed a stronger contractile force than that derived using heart-derived type III collagen, type V collagen, or without collagen (Fig. 6B and S7B).

Next, we calculated the contraction duration (CD) and relaxation duration (RD) (Fig. S7C). hiPSC-EHT obtained using heart-derived type III collagen showed significantly lower RD/CD ratios, indicating that the heart-derived type III collagen promoted efficient relaxation (Fig. 6C and S7D). Therefore, Hc-EHT showed a significantly lower RD/CD ratio than Sc-EHT (Fig. 6D). RD/CD_{80} and RD/CD_{50} showed similar trends (Fig. S7E). At the same time, Hc-EHT exhibited a stronger contractile force than Sc-EHT, whereas no difference in contractile force was observed compared to hiPSC-EHT without collagen, albeit an increased trend was noted (Fig. 6E). Hc-EHT and Sc-EHT showed a higher beating rate than hiPSC-EHT without collagen (Fig. 6F). We also analyzed the contraction and relaxation profiles of dissociated CMs obtained from hiPSC-EHT four weeks post-EHT formation. Calcium transient analysis of dissociated CMs demonstrated that CMs from Hc-EHT had a shorter time to 50% decay than CMs from Sc-EHT and hiPSC-EHT without collagen, and times to peak did not significantly differ (Figs. S7F and

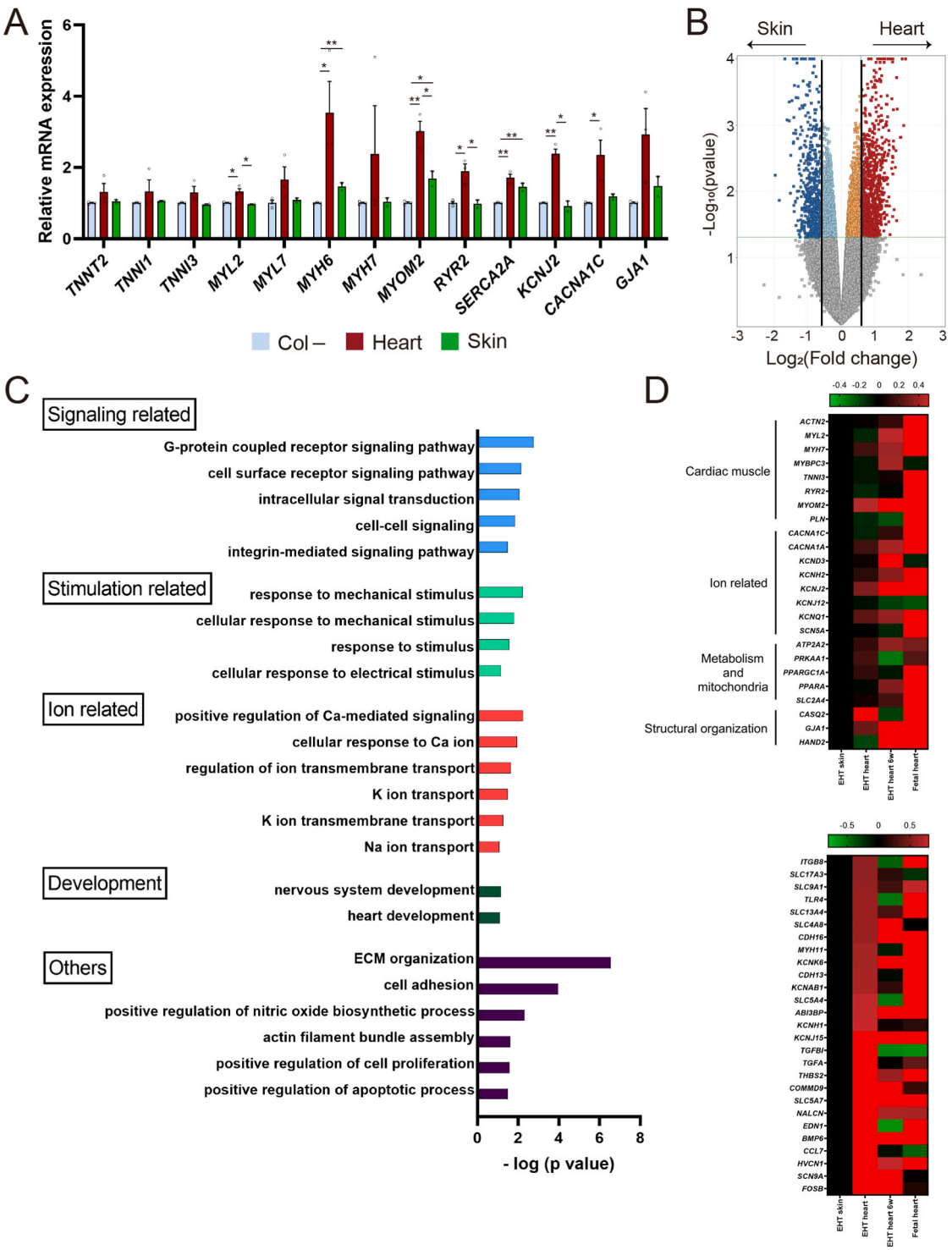

Fig. 3. Heart-derived collagen promotes cardiac genetic maturation of human induced pluripotent stem cell-derived (hiPSC) engineered heart tissue (EHT)
(A) qRT-PCR showing enrichment at 4 weeks of cardiac muscle-related and ion-related genes in hiPSC-EHT generated without collagen or using heart or skin collagen (n = 3). mRNA expression of hiPSC-EHT generated without collagen was defined as the control value. Differences between each group were regarded as significant at $p < 0.05$
(B) Volcano plot showing genes with differential expression (fold change >1.5), at 3 weeks, between heart collagen-derived (Hc)-EHT and skin collagen-derived (Sc)-EHT, based on microarray analyses (n = 3 independent biological replicates). Genes significantly up- and downregulated in Hc-EHT relative to Sc-EHT are highlighted in red and blue, respectively
(C) GO analyses of the upregulated genes in Hc-EHT relative to Sc-EHT at 3 weeks. GO groups were considered significant using a p-value cut-off of 0.05
(D) Heatmap of fold change of maturation-related genes (upper panel) and genes upregulated in Hc-EHT relative to Sc-EHT (lower panel) (n = 3 independent biological replicates for Hc-EHT and Sc-EHT at 3 weeks; n = 1 sample for Hc-EHT at 6 weeks, and fetal heart). The scales extend from −0.5 to +0.5 on the $\log_2$ scale (upper panel) and from −0.8 to +0.8 on the $\log_2$ scale (lower panel), as indicated at the top of each image
All data are presented as mean ± SEM; $*p < 0.05$, $**p < 0.01$. (For interpretation of the references to colour in this figure legend, the reader is referred to the Web version of this article.)

Table 2
GSEA analysis of upregulated genes in EHTs with heart-derived collagen.

Classification	Gene set	NES	Nominal p-value	Analyze method
CM	ventricular cardiac muscle cell action potential	1.677	0	BP
	cardiac muscle cell action potential	1.62	0.008	BP
	cardiac muscle cell action potential involved in contraction	1.486	0.004	BP
	cardiac muscle cell contraction	1.389	0.027	BP
	cardiac muscle contraction	1.324	0	BP
Conduction	ATPase coupled ion transmembrane transporter activity	1.618	0.005	MF
	cardiac conduction system development	1.573	0.003	BP
	cardiac conduction	1.558	0	BP
	cell communication involved in cardiac contraction	1.536	0.003	BP
Metabolism	ATP biosynthetic process	1.743	0	BP
	mitochondrial respiratory chain complex assembly	1.742	0	BP
ECM, adhesion	cell cell contact zone	1.414	0.015	CC
	ECM receptor interaction	1.311	0.049	KEGG
Proliferation	cell cycle	1.284	0.033	KEGG
Development	regulation of embryonic development	1.772	0	BP

NES; normalized edrichment score, BP; binding protein, CC; cellular component, KEGG; KEGG gene sets, MF; molecular function.

S7G). We also confirmed that CMs from Hc-EHT had a higher amplitude than CMs from hiPSC-EHT without collagen, and no difference in peak amplitude was observed compared with CMs from Sc-EHT, albeit an increased trend was noted (Fig. S7G).

We quantified hiPSC-EHT type I and III collagens content of hiPSC-EHT 4 weeks after generation. In this process, we generated hiPSC-EHT using each type collagen with purified hiPSC-CMs and human CFs, instead of porcine CFs, to determine whether the resulting collagen in the EHT is of native or cellular origin. We calculated collagen levels of porcine-derived native (included when generating hiPSC-EHT) collagen and human-derived (hiPSC-CMs and human CFs derived) collagen by using human- and porcine-specific marker peptides (Fig. S8A). First, based on comparison of hiPSC-EHT generated using crude collagen with and without cells (= Ctrl), incubating the EHT for 4 weeks reduced collagen content by more than half (85.96 μg/mg vs. 31.90 μg/mg) (Fig. S8B). Notably, hiPSC-EHT generated using purified type III or V collagen contained more collagen than that generated using type I and crude collagen, indicating that type I collagen was more susceptible to degradation than types III and V (Fig. S8B). In contrast, the proportions of type I and III collagens (3:1 to 4:1) in hiPSC-EHT generated using crude collagen with or without cells were unchanged after 4 weeks of culture (Fig. S8C). Although hiPSC-EHT generated using type V collagen, or without collagen, produced more type I collagen than hiPSC-EHT generated using type I, type III and crude collagens, human origin cell-derived collagen was produced far less than porcine-derived native collagen (Figs. S8C and S8D). Further, hiPSC-EHT generated without collagen contained more type I collagen, indicating that including native type I and type III collagens reduced *de novo* collagen production by human stromal cells (Fig. S8D). These results indicate that hiPSC-EHT generated using collagen retains the features of native collagen after long-term incubation.

To identify which component of heart collagen most strongly promotes maturation, we conducted qRT-PCR analyses at 4 weeks. The expression of CM-related genes and ion channel-related genes was higher in EHT generated using heart-derived crude collagen than in that generated using purified collagen (Fig. 6G). Finally, we confirmed that both type I collagen and type III collagen were necessary to mature the EHT. Supplementing heart-derived type III collagen (final content ratio; 33%) with skin-derived type I collagen significantly reduced the RD/CD ratio; similarly, supplementing skin-derived type III collagen with skin-derived type I collagen reduced the RD/CD ratio (Fig. 6H and Fig. S8E). The expression of CM-and ion channel-related genes was higher in EHT generated using both skin-derived type I and III collagen than that generated using purified skin-derived type I or type III collagen (Fig. 6I). Notably, the expression of CM-and ion channel-related genes was upregulated more strongly by the use of heart-derived type III collagen than by that of skin-derived type III collagen (Fig. 6I). Supplementation with heart-derived type V collagen (final content ratio; 10%) did not significantly alter the RD/CD ratio, but did partially upregulate the expression of CM- and ion channel-related genes (Fig. 6H, Figs. S8E and 6I). Overall, supplementing type III and type V collagens with skin-derived type I collagen did not significantly alter the contraction force of hiPSC-EHT (Fig. S8F). Thus, tissue maturation may be significantly affected by the type and distribution of collagen present in the tissue.

4. Discussion

This study aimed to elucidate the impact of the ECM, and particularly of collagen, in heart tissue engineering. We found that heart-derived collagen was the most suitable for retaining the contracted tissue shape in our EHT system. Using heart-derived collagen promoted functional and structural maturation of heart tissue more than skin-derived collagen. EHT generated using heart-derived collagen exhibited stronger contraction and faster relaxation than EHT generated using skin-derived collagen (Fig. 7). Our mRNA and transcriptome analyses revealed that the upregulation of maturation-related genes was accompanied by upregulation of signaling pathways related to mechanical stimulation, activation of various signaling pathways, and ion transport. In addition, our findings reveal that the differences in the content rate of fibrillar collagen composition, leading to differences in the characteristics of collagen fibrils, play significant roles in the superiority of heart-derived collagen in shape retention and maturation. Finally, we demonstrated that skin-derived collagen could improve the shape retention and maturation by changing the fibrillar collagen composition. We believe that these findings will open new avenues in the engineering of ideal heart tissue. This is the first study to demonstrate the effects of organ-derived collagen, and the different collagen types in tissue engineering.

Although differences in collagen-type composition between organs and disease phenotypes have been reported, little is known about their impacts on tissue function. At least 29 types of collagen have been described in detail, and their structural diversity is reflected by differences in their cell-adhesive sequences [50,51]. Previous studies have reported the distribution of these sequences in fibrillar collagen, and their resulting affinities to supporting integrin ligation and cell types [52]. Heart collagens have ligand sites that have the potential to promote cellular activity extensively during heart development and regeneration. Fibrillar collagens are known to provide elasticity and structural integrity to heart tissue. Fibrillar collagens interact with integrins, thus maintaining myocardial shape, thickness, and stiffness by mediating cellular adhesion in collaboration with CFs [32,53–55]. Although heart ECM is conventionally reported to consist of approximately 75%–80% fibrillar collagens, mainly type I (85%) and type III (15%), with up to 5% of type V, our results revealed a larger proportion of type III collagen [55,56]. This discrepancy can be attributed to differences in the developmental stage of the heart, the study species, and the quantification methods.

Our results highlight the importance of type III collagen in heart tissue engineering. Notably, our results reveal that type I collagen is advantageous for strong contraction and that type III collagen is advantageous for efficient relaxation and shape retention. These trends may be consistent with previous studies which have reported that

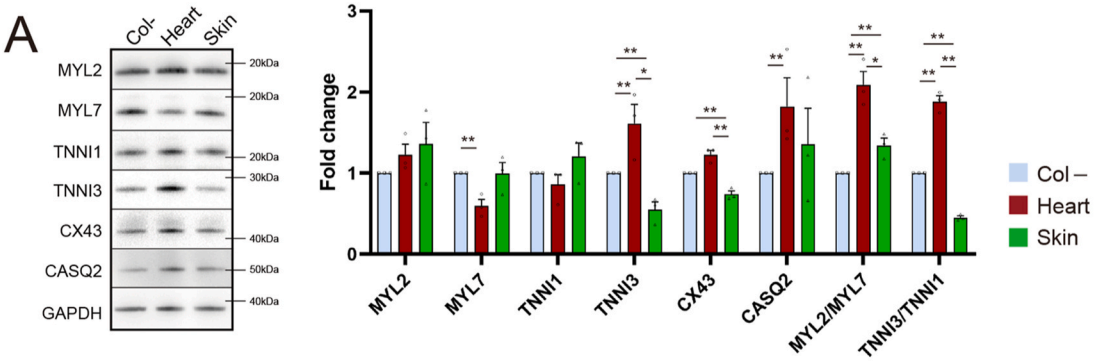

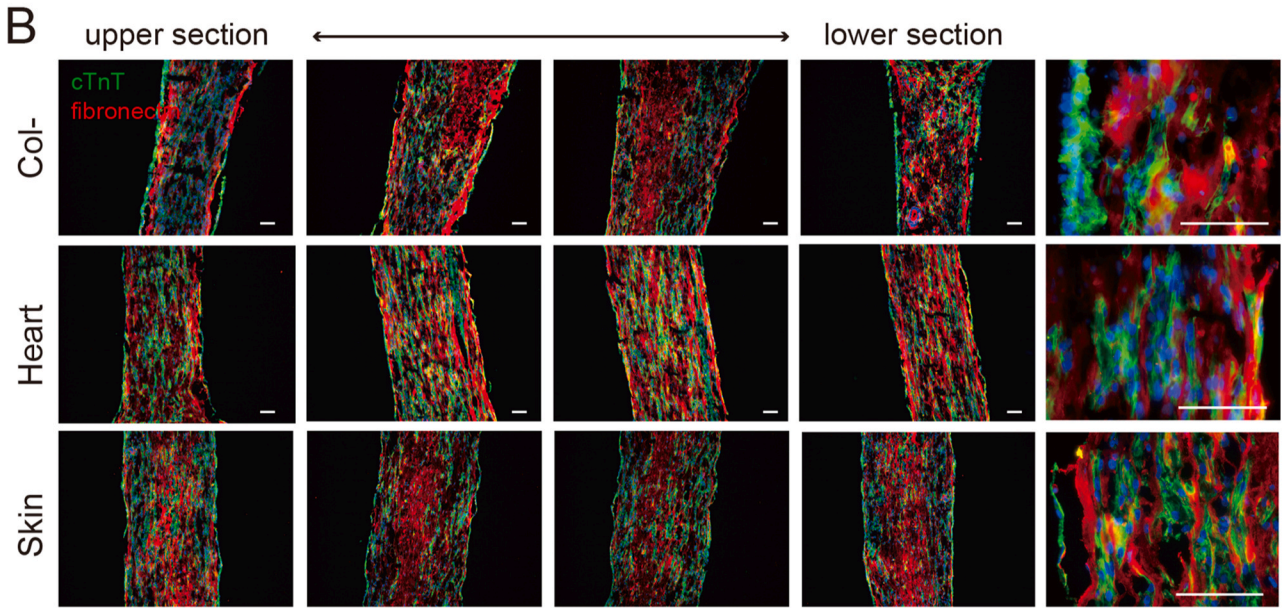

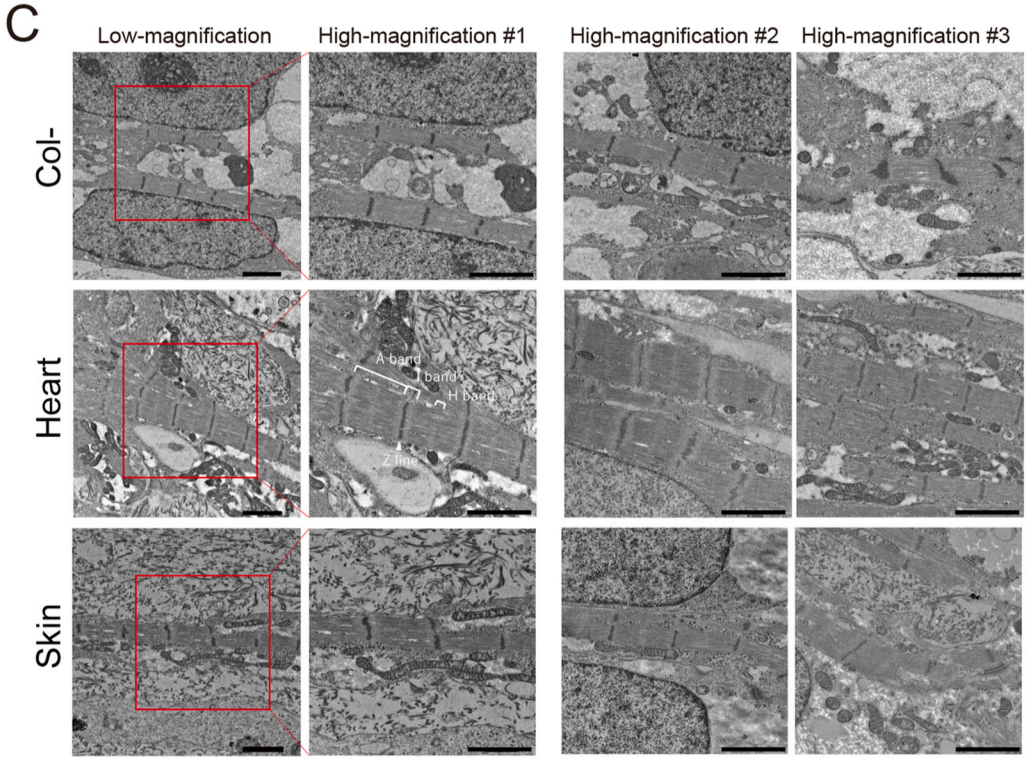

(caption on next page)

Fig. 4. Heart-derived collagen promotes cardiac structural maturation of human induced pluripotent stem cell-derived (hiPSC) engineered heart tissue (EHT)
(A) Representative Western blot images at 4 weeks of hiPSC-EHT generated without collagen, using heart-derived collagen (Hc)-EHT, or using skin collagen-derived (Sc)-EHT, and quantification of protein content relative to that of GAPDH (n = 3). Differences between each group were regarded as significant at $p < 0.05$
(B) Immunofluorescent staining for cTnT (green), fibronectin (red), and nuclei (blue, DAPI). Scale bars represent 200 μm
(C) Representative transmission electron microscope images of sarcomere structures in hiPSC-EHT generated without collagen, Hc-EHT, and Sc-EHT, at 4 weeks. The bands (A, I, and H), and the Z line, are highlighted for the Hc-EHT sample. Scale bars represent 2 μm. (For interpretation of the references to colour in this figure legend, the reader is referred to the Web version of this article.)

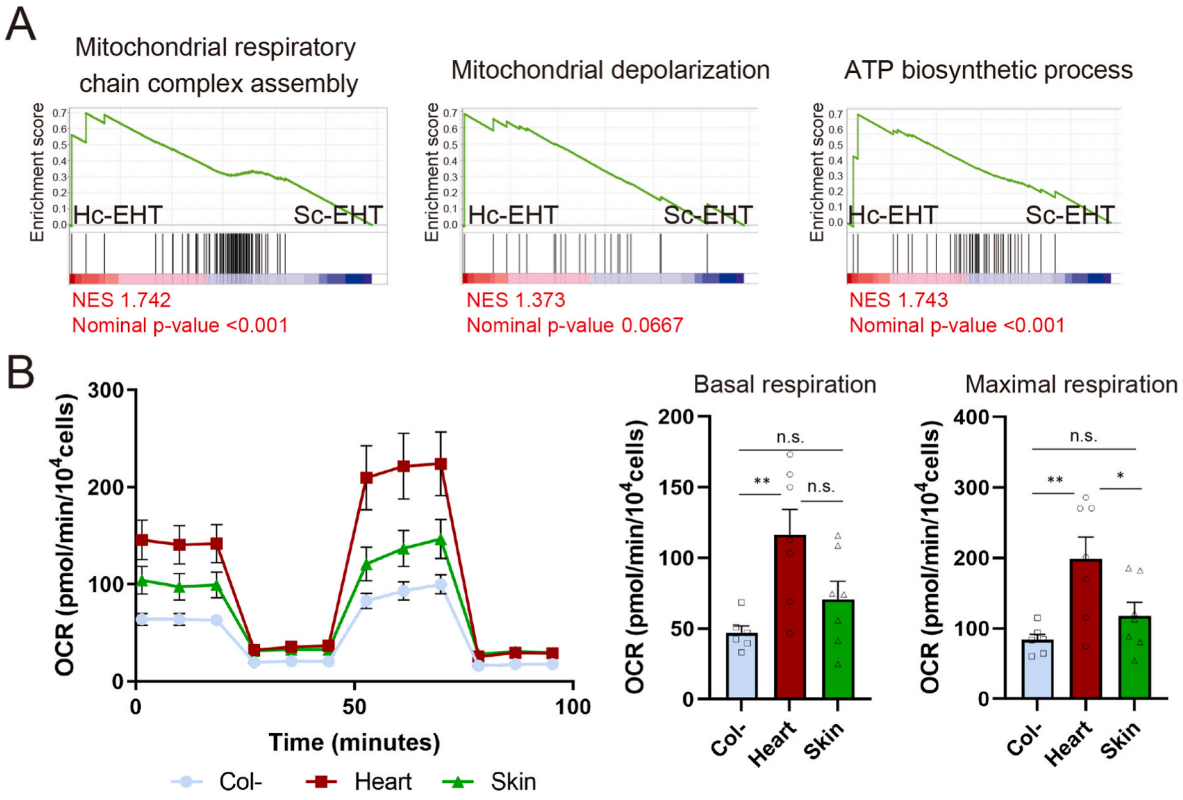

Fig. 5. Heart-derived collagen promotes cardiac functional maturation of human induced pluripotent stem cell-derived (hiPSC) engineered heart tissue (EHT)
(A) Enrichment score plot of the mitochondrial respiratory chain complex assembly, ATP biosynthetic process, and mitochondrial depolarization gene set. NES; normalized enrichment score
(B) Representative traces responding to oligomycin, carbonyl cyanide 4-(trifluoromethoxy) phenylhydrazone (FCCP), and rotenone/antimycin A, and statistical analyses of oxygen consumption rate (OCR) for basal and maximal respiration of cardiomyocytes dissociated from hiPSC-EHT generated without collagen, in heart-derived collagen (Hc)-EHT, and in skin collagen-derived (Sc)-EHT, at 4 weeks (each n ≧ 6). Differences between each group were regarded as significant at $p < 0.05$
All data are presented as mean ± SEM; $*p < 0.05$, $**p < 0.01$.

fibrosis in myocardial infarction, cardiomyopathy, and atrial fibrillation involves an increase in the proportion of fibrillar collagen, with a small shift in favor of type I and type III collagen; further, neonatal hearts, which have a higher ratio of types I and III collagen than postnatal hearts, are poorer compliant [32,57]. Type III collagen plays a significant role in ECM proliferation [32,57,58]. This is consistent with our findings for hiPSC-EHT collagen content, which revealed that type III collagen was less prone to degradation than type I collagen. Moreover, hiPSC-EHT generated using crude heart-derived collagen was more mature than that generated using purified type I, III, and V collagens. This result indicates the importance of interactions between the collagen types and the ratios of heart-derived collagen types [59]. Further, heart-derived collagen has non-negligible levels of type V collagen. Type V collagen has been underestimated because of its rarity and the lack of accurate quantitative methods. Nonetheless, it is believed to be necessary for myocardial morphogenesis and heart-valve development, and its role as a critical driver of ECM production after injury has been recently reported [60–62]. As our findings reveal that type V content was highest in the left ventricle, but negligible in other organs, type V collagen may play a significant role in the maintenance of constant cardiac beating. Although type V collagen itself did not significantly affect hiPSC-EHT width or contraction–relaxation function, it may promote maturation as a driver of ECM production, when mixed with types I and III. As a limitation of this study, owing to the difficulty of obtaining a sufficient quantity of purified heart type V collagen, we could not fully examine the difference between type III and V collagens,

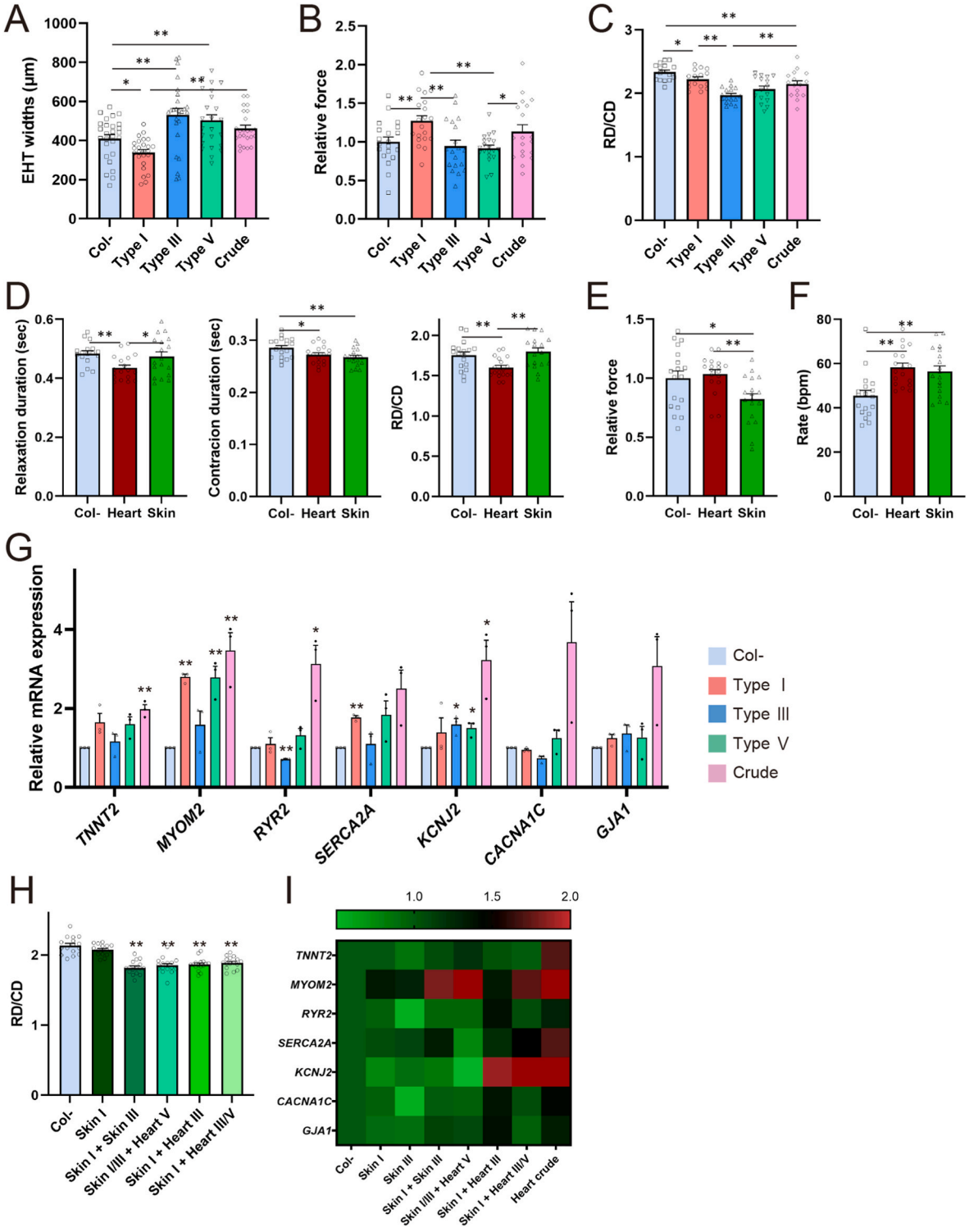

(caption on next page)

Fig. 6. Heart collagen induces more mature contraction–relaxation status in human induced pluripotent stem cell-derived (hiPSC) engineered heart tissue (EHT) by providing abundant collagen type III
(A) The widths at 2 weeks of hiPSC-EHT generated using heart-derived type I, III, V collagens, crude collagen, and without collagen, measured by microscopy (each n ≧ 18/3)
(B) Relative contractile force at 3 weeks of hiPSC-EHT generated using heart-derived type I, III, V collagens, crude collagen, and without collagen (each n ≧ 18/3). The average contractile force at 3 weeks of hiPSC-EHT generated without collagen was defined as the control value
(C) Ratios of relaxation duration (RD) to contraction duration (CD) of hiPSC-EHT generated using heart-derived type I, III, V collagens, crude collagen, and without collagen, at 3 weeks (each n ≧ 18/3)
(D) RD, CD, and the RD/CD ratio of heart-derived collagen (Hc)-EHT, skin collagen-derived (Sc)-EHT, and hiPSC-EHT generated without collagen, at 3 weeks (each n ≧ 18/3)
(E) Relative force of Hc-EHT, Sc-EHT, and hiPSC-EHT generated without collagen, at 3 weeks (each n ≧ 18/3). The average contractile force at 3 weeks of hiPSC-EHT generated without collagen was defined as the control value
(F) Beating rate of Hc-EHT, Sc-EHT, and hiPSC-EHT generated without collagen at 3 weeks (each n ≧ 18/3)
(G) qRT-PCR showing enrichment of cardiac muscle- and ion-related genes in hiPSC-EHT generated without collagen, and in hiPSC-EHT generated using each type of fibrillar heart collagen, at 4 weeks (n = 3). mRNA expression of hiPSC-EHT generated without collagen was defined as relative control. Differences between hiPSC-EHT generated without collagen and those generated using heart-derived collagen types were regarded as significant
(H) The RD/CD ratio of hiPSC-EHT generated using skin-derived type I collagen, skin-derived type I + III collagen (each content ratio; 67% + 33%), skin-derived type I + III + heart-derived type V collagen (60% + 30% + 10%), skin-derived type I + heart-derived type III collagen (67% + 33%), skin-derived type I + heart-derived type III + V collagen (60% + 30% + 10%), and without collagen, at 3 weeks (each n ≧ 16/3). Differences between hiPSC-EHT generated without collagen and with other types collagens were regarded as significant
(I) Heatmap showing mRNA expression of cardiac muscle- and ion-related genes of hiPSC-EHT generated with skin-derived type I collagen, skin-derived type I + III collagen, skin-derived type I + III + heart-derived type V collagen, skin-derived type I + heart-derived type III collagen, skin-derived type I + heart-derived type III + type V collagen, and without collagen at 4 weeks (n = 3). mRNA expression of hiPSC-EHT generated without collagen was defined as the control value
Replicates are indicated as EHT samples/number of independent experiments
All data are presented as mean ± SEM; $*p < 0.05$, $**p < 0.01$, vs. the control.

which have similar trends in shape retention (Fig. 2F). Further intensive studies may be warranted. As another limitation of this study, we were unable to elucidate the mechanisms underlying the different effects of using collagen of the same type from different organs. Although the kidney, liver, lung, and skin exhibited similar fibrillar collagen content, their collagen differed in turbidity, fibrillogenesis, and fibril thickness (Fig. 2A–C). Adjusting the levels of skin-derived type I and III collagen did not fully improve the maturity of hiPSC-EHT (Fig. 6H). Our study has focused entirely on differences in collagen type. Post-translational modifications in collagens are known to vary substantially between organs [51,63–65]. Future studies of post-translational qualitative and quantitative changes in each organ-derive purified type I and III collagens may provide further insight into these differences.

Furthermore, we evaluated fibril formation for each collagen type. To the best of our knowledge, this is the first study to compare the characteristics and functions of collagen fibrils from various porcine organs. Notably, heart collagens exhibited opposite trends in fibril formation compared to skin collagens; this is consistent with the shape-retaining ability of hiPSC-EHT. In addition, because type III collagen exhibited low turbidity and fine fibers, hiPSC-EHT generated using type III collagen had wide EHT widths and efficient shape retention. However, although it may be reasonable that heart and spleen collagen, which contain a large proportion of type III collagen, showed low turbidity, kidney collagen, which does not contain so much type III collagen, also showed low turbidity. Since the characteristics of type I collagen would differ between organs, further analysis may be necessary.

We evaluated contractile function by measuring the distances between the attachment points and relaxation function by calculating the durations of contraction and relaxation. Although these parameters can be substantially affected by differences in measurement conditions (auxotonic vs isometric), media, and beating rates, we did not consider differences in these conditions, altering only the collagen conditions [66,67]. Moreover, by simultaneously inducing a large number of purified hiPSC-CMs via metabolic selection, we were able to avoid lot-to-lot variation in hiPSC-CMs and achieve stable data collection [38–40,68,69].

We first attempted hiPSC-EHT generation without Matrigel, because using Matrigel has several drawbacks, such as being derived from mouse sarcoma cells, having complex and poorly defined components, and exhibiting lot-to-lot variations [70]. In contrast, collagen has several advantages in terms of its biocompatibility, biodegradability, low antigenicity, high purity, and low cost [52]. Here, EHT generated using heart-derived collagen exhibited better, but not perfect, shape retention than other organs-derived collagen. Matrigel achieved substantially better shape retention, indicating the importance of type IV and basement membrane collagen in tissue engineering. Via LC-MS, we confirmed that Matrigel contains collagen type IV, laminin-111, and Nidogen-1. Because commercially available laminin 221 and laminin 511 E8 fragment could not completely substitute for Matrigel, we generated hiPSC-EHT using a mixture of fibrillar collagen and Matrigel at half of the conventional concentration [41]. Further analysis and developments in handling basement membrane collagen may help to resolve these challenges.

In summary, these findings reveal the effectiveness of heart-derived collagen in heart tissue engineering. Heart-derived collagen contains more abundant type III and V collagen, and EHT generated from heart-derived collagen exhibited maturation and efficient contraction–relaxation kinetics. Further studies and analyses will help to develop heart-derived collagen as a standard for heart tissue engineering.

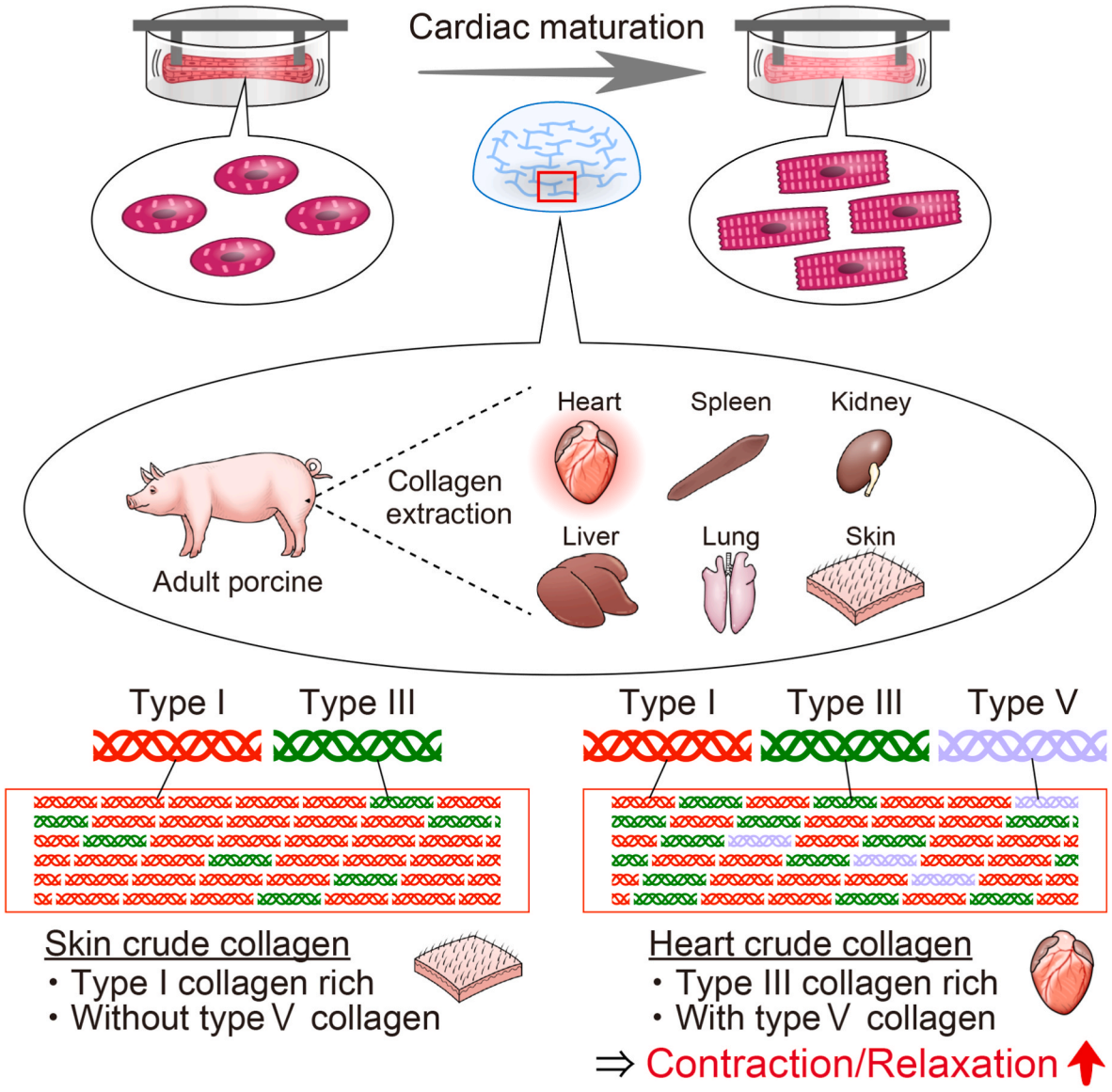

Fig. 7. Study summary
Heart-derived collagen induces cardiac maturation and better contraction–relaxation status in human induced pluripotent stem cell-derived (hiPSC) engineered heart tissue (EHT) than collagen from other organs. This suggests the importance of collagen types III and V, which are relatively abundant in the heart.

Credit author statement

Hidenori Tani: Conceptualization, Methodology, Investigation, Discussion, Writing- Original draft preparation and Editing. Eiji Kobayashi: Conceptualization, Discussion, Supervision. Shinomi Yagi: Investigation, Discussion. Keisuke Tanaka: Discussion, Supervision. Kotaro Kameda-Haga: Investigation, Discussion, Data curation. Shinsuke Shibata: Investigation, Discussion, Supervision. Nobuko Moritoki: Investigation, Discussion. Kaworu Takatsuna: Investigation, Discussion. Taijun Moriwaki: Investigation, Discussion. Otoya Sekine: Investigation, Discussion. Tomohiko Umei: Investigation, Discussion. Yuika Morita: Investigation, Discussion. Yusuke Soma: Investigation, Discussion. Yoshikazu Kishino: Investigation, Discussion. Yujiro Kawai: Investigation, Discussion. Hideaki Kanazawa: Discussion, Supervision. Jun Fujita: Discussion, Supervision. Shunji Hattori: Discussion, Supervision. Keiichi Fukuda: Discussion, Supervision. Shugo Tohyama: Conceptualization, Methodology, Discussion, Writing- Reviewing and Editing, Supervision.

Funding

This work was supported by an AMED grant (JP22bm1123010 to S. T.), JSPS KAKENHI (Grant 20H03768 and 20H05744 to S.T. and 19H03660 to J.F.), KISTEC grant (to S.T.), a Japan Heart Foundation Research Grant (to H.T.) and a research grant from Heartseed Inc.

Declaration of competing interest

The authors declare the following financial interests/personal relationships which may be considered as potential competing interests: S. T. is an advisor of Heartseed, Inc. K.F. is a co-founder and CEO of Heartseed, Inc. H.K., J.F., K.F., and S.T. own equity in Heartseed Inc. The remaining authors declare no competing interests.

Data availability

Data will be made available on request.

Acknowledgments

We thank DNA Chip Research Inc. for microarray analysis. We are grateful to Tomomi Kiriyama-Tanaka, Yuki Taga, and Kazunori Mizuno (Nippi Research Institute of Biomatrix) for their kind support and discussions. We thank Yoshiko Miyake, Tomoko Haruna, Rei Ohno, Yuki Yamamoto, Sayaka Kanaami, Noriko Kabasawa, Kuniko Momoi, Yui Narita, Yumeko Konno, and Shuta Minagawa (Department of Cardiology, Keio University) for technical assistance with cell preparation and culture.

Appendix A. Supplementary data

Supplementary data to this article can be found online at https://doi.org/10.1016/j.biomaterials.2023.122174.

References

[1] W.H. Zimmermann, K. Schneiderbanger, P. Schubert, M. Didié, F. MüNzel, J. F. Heubach, S. Kostin, W.L. Neuhuber, T. Eschenhagen, Tissue engineering of a differentiated cardiac muscle construct, Circ. Res. 90 (2002) 223–230, https://doi.org/10.1161/hh0202.103644.

[2] A. Hansen, A. Eder, M. Bonstrup, M. Flato, M. Mewe, S. Schaaf, B.L. Aksehirlioglu, A. SchwoRer, J. Uebeler, T. Eschenhagen, Development of a drug screening platform based on engineered heart tissue, Circ. Res. 107 (1) (2010) 35–44, https://doi.org/10.1161/CIRCRESAHA.109.211458.

[3] M.N. Hirt, J. Boeddinghaus, A. Mitchell, S. Schaaf, C. Börnchen, C. Müller, H. Schulz, N. Hubner, J. Stenzig, A. Stoehr, C. Neuber, A. Eder, P.K. Luther, A. Hansen, T. Eschenhagen, Functional improvement and maturation of rat and human engineered heart tissue by chronic electrical stimulation, J. Mol. Cell. Cardiol. 74 (2014) 151–161, https://doi.org/10.1016/j.yjmcc.2014.05.009.

[4] A. Eder, I. Vollert, A. Hansen, T. Eschenhagen, Human engineered heart tissue as a model system for drug testing, Adv. Drug Deliv. Rev. 96 (2016) 214–224, https://doi.org/10.1016/j.addr.2015.05.010.

[5] M.D. Lemoine, I. Mannhardt, K. Breckwoldt, M. Prondzynski, F. Flenner, B. Ulmer, M.N. Hirt, C. Neuber, A. Horváth, B. Kloth, H. Reichenspurner, S. Willems, A. Hansen, T. Eschenhagen, T. Christ, Human iPSC-derived cardiomyocytes cultured in 3D engineered heart tissue show physiological upstroke velocity and sodium current density, Sci. Rep. 7 (2017) 5464, https://doi.org/10.1038/s41598-017-05600-w.

[6] I. Mannhardt, A. Eder, B. Dumotier, M. Prondzynski, E. Krämer, M. Traebert, K. D. Söhren, F. Flenner, K. Stathopoulou, M.D. Lemoine, L. Carrier, T. Christ, T. Eschenhagen, A. Hansen, Blinded contractility analysis in hiPSC-cardiomyocytes in engineered heart tissue format: comparison with human atrial trabeculae, Toxicol. Sci. 158 (2017) 164–175, https://doi.org/10.1093/toxsci/kfx081.

[7] B.M. Ulmer, A. Stoehr, M.L. Schulze, S. Patel, M. Gucek, I. Mannhardt, S. Funcke, E. Murphy, T. Eschenhagen, A. Hansen, Contractile work contributes to maturation of energy metabolism in hiPSC-derived cardiomyocytes, Stem Cell Rep. 10 (2018) 834–847, https://doi.org/10.1016/j.stemcr.2018.01.039.

[8] U. Saleem, B.J. van Meer, P.A. Katili, , N.A.N.Mohd. Mohd Yusof, I. Mannhardt, A. K. Garcia, L. Tertoolen, T. de Korte, M.L.H. Vlaming, K. McGlynn, J. Nebel, A. Bahinski, K. Harris, E. Rossman, X. Xu, F.L. Burton, G.L. Smith, P. Clements, C. L. Mummery, T. Eschenhagen, A. Hansen, C. Denning, Blinded, multicenter evaluation of drug-induced changes in contractility using human-induced pluripotent stem cell-derived cardiomyocytes, Toxicol. Sci. 176 (2020) 103–123, https://doi.org/10.1093/toxsci/kfaa058.

[9] F. Cuello, A.E. Knaust, U. Saleem, M. Loos, J. Raabe, D. Mosqueira, S. Laufer, M. Schweizer, P. van der Kraak, F. Flenner, B.M. Ulmer, I. Braren, X. Yin, K. Theofilatos, J. Ruiz-Orera, G. Patone, B. Klampe, T. Schulze, A. Piasecki, Y. Pinto, A. Vink, N. Hübner, S. Harding, M. Mayr, C. Denning, T. Eschenhagen, A. Hansen, Impairment of the ER/mitochondria compartment in human cardiomyocytes with PLN p.Arg14del mutation, EMBO Mol. Med. 13 (2021), e13074, https://doi.org/10.15252/emmm.202013074.

[10] S.F. Badylak, The extracellular matrix as a biologic scaffold material, Biomaterials 28 (2007) 3587–3593, https://doi.org/10.1016/j.biomaterials.2007.04.043.

[11] O. Pagliarosi, V. Picchio, I. Chimenti, E. Messina, R. Gaetani, Building an artificial cardiac microenvironment: a focus on the extracellular matrix, Front. Cell Dev. Biol. 8 (2020), 559032, https://doi.org/10.3389/fcell.2020.559032.

[12] M. Tiburcy, J.E. Hudson, P. Balfanz, S. Schlick, T. Meyer, M.L. Chang Liao, E. Levent, F. Raad, S. Zeidler, E. Wingender, J. Riegler, M. Wang, J.D. Gold, I. Kehat, E. Wettwer, U. Ravens, P. Dierickx, L.W. Van Laake, M.J. Goumans, S. Khadjeh, K. Toischer, G. Hasenfuss, L.A. Couture, A. Unger, W.A. Linke, T. Araki, B. Neel, G. Keller, L. Gepstein, J.C. Wu, W.H. Zimmermann, Defined engineered human myocardium with advanced maturation for applications in heart failure modeling and repair, Circulation 135 (2017) 1832–1847, https://doi.org/10.1161/CIRCULATIONAHA.116.024145.

[13] W. Zhang, C.W. Kong, M.H. Tong, W.H. Chooi, N. Huang, R.A. Li, B.P. Chan, Maturation of human embryonic stem cell-derived cardiomyocytes (hESC-CMs) in 3D collagen matrix: effects of niche cell supplementation and mechanical stimulation, Acta Biomater. 49 (2017) 204–217, https://doi.org/10.1016/j.actbio.2016.11.058.

[14] J. Schwan, A.T. Kwaczala, T.J. Ryan, O. Bartulos, Y. Ren, L.R. Sewanan, A. H. Morris, D.L. Jacoby, Y. Qyang, S.G. Campbell, Anisotropic engineered heart tissue made from laser-cut decellularized myocardium, Sci. Rep. 6 (2016), 32068, https://doi.org/10.1038/srep32068.

[15] R. Ng, L.R. Sewanan, A.L. Brill, P. Stankey, X. Li, Y. Qyang, B.E. Ehrlich, S. G. Campbell, Contractile work directly modulates mitochondrial protein levels in human engineered heart tissues, Am. J. Physiol. Heart Circ. Physiol. 318 (2020) H1516–H1524, https://doi.org/10.1152/ajpheart.00055.2020.

[16] P.M. Crapo, T.W. Gilbert, S.F. Badylak, An overview of tissue and whole organ decellularization processes, Biomaterials 32 (2011) 3233–3243, https://doi.org/10.1016/j.biomaterials.2011.01.057.

[17] Q. Wang, H. Yang, A. Bai, W. Jiang, X. Li, X. Wang, Y. Mao, C. Lu, R. Qian, F. Guo, T. Ding, H. Chen, S. Chen, J. Zhang, C. Liu, N. Sun, Functional engineered human cardiac patches prepared from nature's platform improve heart function after acute myocardial infarction, Biomaterials 105 (2016) 52–65, https://doi.org/10.1016/j.biomaterials.2016.07.035.

[18] C. Yu, X. Ma, W. Zhu, P. Wang, K.L. Miller, J. Stupin, A. Koroleva-Maharajh, A. Hairabedian, S. Chen, Scanningless and continuous 3D bioprinting of human tissues with decellularized extracellular matrix, Biomaterials 194 (2019) 1–13, https://doi.org/10.1016/j.biomaterials.2018.12.009.

[19] J.H. Tsui, A. Leonard, N.D. Camp, J.T. Long, Z.Y. Nawas, R. Chavanachat, A.S. T. Smith, J.S. Choi, Z. Dong, E.H. Ahn, A. Wolf-Yadlin, C.E. Murry, N.J. Sniadecki, D.H. Kim, Tunable electroconductive decellularized extracellular matrix hydrogels for engineering human cardiac microphysiological systems, Biomaterials 272 (2021), 120764, https://doi.org/10.1016/j.biomaterials.2021.120764.

[20] C. Williams, E. Budina, W.L. Stoppel, K.E. Sullivan, S. Emani, S.M. Emani, L. D. Black 3rd, Cardiac extracellular matrix-fibrin hybrid scaffolds with tunable properties for cardiovascular tissue engineering Black, Acta Biomater. 14 (2015) 84–95, https://doi.org/10.1016/j.actbio.2014.11.035.

[21] A.J. Engler, S. Sen, H.L. Sweeney, D.E. Discher, Matrix elasticity directs stem cell lineage specification, Cell 126 (2006) 677–689, https://doi.org/10.1016/j.cell.2006.06.044.

[22] S. Kurotsu, T. Sadahiro, R. Fujita, H. Tani, H. Yamakawa, F. Tamura, M. Isomi, H. Kojima, Y. Yamada, Y. Abe, Y. Murakata, T. Akiyama, N. Muraoka, I. Harada, T. Suzuki, K. Fukuda, M. Ieda, Soft matrix promotes cardiac reprogramming via inhibition of YAP/TAZ and suppression of fibroblast signatures, Stem Cell Rep. 15 (2020) 612–628, https://doi.org/10.1016/j.stemcr.2020.07.022.

[23] A.J. Engler, C. Carag-Krieger, C.P. Johnson, M. Raab, H.Y. Tang, D.W. Speicher, J. W. Sanger, J.M. Sanger, D.E. Discher, Embryonic cardiomyocytes beat best on a matrix with heart-like elasticity: scar-like rigidity inhibits beating, J. Cell Sci. 121 (2008) 3794–3802, https://doi.org/10.1242/jcs.029678.

[24] J.L. Young, A.J. Engler, Hydrogels with time-dependent material properties enhance cardiomyocyte differentiation in vitro, Biomaterials 32 (2011) 1002–1009, https://doi.org/10.1016/j.biomaterials.2010.10.020.

[25] J.L. Young, K. Kretchmer, M.G. Ondeck, A.C. Zambon, A.J. Engler, Mechanosensitive kinases regulate stiffness-induced cardiomyocyte maturation, Sci. Rep. 4 (2014) 6425, https://doi.org/10.1038/srep06425.

[26] Y.R. Shih, K.F. Tseng, H.Y. Lai, C.H. Lin, O.K. Lee, Matrix stiffness regulation of integrin-mediated mechanotransduction during osteogenic differentiation of human mesenchymal stem cells, J. Bone Miner. Res. 26 (2011) 730–738, https://doi.org/10.1002/jbmr.278.

[27] J.R. Gershlak, L.D. Black, Beta 1 integrin binding plays a role in the constant traction force generation in response to varying stiffness for cells grown on mature cardiac extracellular matrix, Exp. Cell Res. 330 (2015) 311–324, https://doi.org/10.1016/j.yexcr.2014.09.007.

[28] H. Yuan, B. Marzban, K.K. Kit Parker, Myofibrils in cardiomyocytes tend to assemble along the maximal principle stress directions, J. Biomech. Eng. 139 (2017) 1210101–1210108, https://doi.org/10.1115/1.4037795.

[29] D.M. Lyra-Leite, A.M. Andres, A.P. Petersen, N.R. Ariyasinghe, N. Cho, J.A. Lee, R. A. Gottlieb, M.L. McCain, Mitochondrial function in engineered cardiac tissues is regulated by extracellular matrix elasticity and tissue alignment, Am. J. Physiol. Heart Circ. Physiol. 313 (2017) H757–H767, https://doi.org/10.1152/ajpheart.00290.2017.

[30] A. Körner, M. Mosqueira, M. Hecker, N.D. Ullrich, Substrate stiffness influences structural and functional remodeling in induced pluripotent stem cell-derived cardiomyocytes, Front. Physiol. 12 (2021), 710619, https://doi.org/10.3389/fphys.2021.710619.

[31] T.D. Johnson, R.C. Hill, M. Dzieciatkowska, V. Nigam, A. Behfar, K.L. Christman, K. C. Hansen, Quantification of decellularized human myocardial matrix: a comparison of six patients, Proteonomics Clin. Appl. 10 (2016) 75–83, https://doi.org/10.1002/prca.201500048.

[32] V. Schwach, R. Passier, Native cardiac environment and its impact on engineering cardiac tissue, Biomater. Sci. 7 (2019) 3566–3580, https://doi.org/10.1039/c8bm01348a.

[33] S. Stanchev, N. Stamenov, V. Kirkov, E. Dzhambazova, D. Nikolov, A. Paloff, Differential collagen expression in kidney and heart during hypertension, Bratisl. Lek. Listy 121 (2020) 73–78, https://doi.org/10.4149/BLL_2020_011.

[34] E. Rezvani Ghomi, N. Nourbakhsh, M. Akbari Kenari, M. Zare, S. Ramakrishna, Collagen-based biomaterials for biomedical applications, J. Biomed. Mater. Res. B Appl. Biomater. 109 (2021) 1986–1999, https://doi.org/10.1002/jbm.b.34881.

[35] B.S. Moura, M.V. Monteiro, L.P. Ferreira, P. Lavrador, V.M. Gaspar, J.F. Mano, Advancing tissue decellularized hydrogels for engineering human organoids, Adv. Funct. Mater. 32 (2022), https://doi.org/10.1002/adfm.202202825.

[36] S.G. Ozcebe, G. Bahcecioglu, X.S. Yue, P. Zorlutuna, Effect of cellular and ECM aging on human iPSC-derived cardiomyocyte performance, maturity and

senescence, Biomaterials 268 (2021), 120554, https://doi.org/10.1016/j.biomaterials.2020.120554.
[37] X. Lian, J. Zhang, S.M. Azarin, K. Zhu, L.B. Hazeltine, X. Bao, C. Hsiao, T.J. Kamp, S.P. Palecek, Directed cardiomyocyte differentiation from human pluripotent stem cells by modulating Wnt/beta-catenin signaling under fully defined conditions, Nat. Protoc. 8 (2013) 162–175, https://doi.org/10.1038/nprot.2012.150.
[38] S. Tohyama, J. Fujita, T. Hishiki, T. Matsuura, F. Hattori, R. Ohno, H. Kanazawa, T. Seki, K. Nakajima, Y. Kishino, M. Okada, A. Hirano, T. Kuroda, S. Yasuda, Y. Sato, S. Yuasa, M. Sano, M. Suematsu, K. Fukuda, Glutamine oxidation is indispensable for survival of human pluripotent stem cells, Cell Metabol. 23 (2016) 663–674, https://doi.org/10.1016/j.cmet.2016.03.001.
[39] S. Tanosaki, T. Akiyama, S. Kanaami, J. Fujita, M.S.H. Ko, K. Fukuda, S. Tohyama, Purification of cardiomyocytes and neurons derived from human pluripotent stem cells by inhibition of de novo fatty acid synthesis, STAR Protoc 3 (2022), 101360, https://doi.org/10.1016/j.xpro.2022.101360.
[40] S. Tohyama, F. Hattori, M. Sano, T. Hishiki, Y. Nagahata, T. Matsuura, H. Hashimoto, T. Suzuki, H. Yamashita, Y. Satoh, T. Egashira, T. Seki, N. Muraoka, H. Yamakawa, Y. Ohgino, T. Tanaka, M. Yoichi, S. Yuasa, M. Murata, M. Suematsu, K. Fukuda, Distinct metabolic flow enables large-scale purification of mouse and human pluripotent stem cell-derived cardiomyocytes, Cell Stem Cell 12 (2013) 127–137, https://doi.org/10.1016/j.stem.2012.09.013.
[41] K. Breckwoldt, D. Letuffe-Brenière, I. Mannhardt, T. Schulze, B. Ulmer, T. Werner, A. Benzin, B. Klampe, M.C. Reinsch, S. Laufer, A. Shibamiya, M. Prondzynski, G. Mearini, D. Schade, S. Fuchs, C. Neuber, E. Krämer, U. Saleem, M.L. Schulze, M. L. Rodriguez, T. Eschenhagen, A. Hansen, Differentiation of cardiomyocytes and generation of human engineered heart tissue, Nat. Protoc. 12 (2017) 1177–1197, https://doi.org/10.1038/nprot.2017.033.
[42] S. Schaaf, A. Eder, I. Vollert, A. Stöhr, A. Hansen, T. Eschenhagen, Generation of strip-format fibrin-based engineered heart tissue (EHT), Methods Mol. Biol. 1181 (2014) 121–129, https://doi.org/10.1007/978-1-4939-1047-2_11.
[43] A. Subramanian, P. Tamayo, V.K. Mootha, S. Mukherjee, B.L. Ebert, M.A. Gillette, A. Paulovich, S.L. Pomeroy, T.R. Golub, E.S. Lander, J.P. Mesirov, Gene set enrichment analysis: a knowledge-based approach for interpreting genome-wide expression profiles, Proc. Natl. Acad. Sci. U.S.A. 102 (2005) 15545–15550, https://doi.org/10.1073/pnas.0506580102.
[44] da W. Huang, B.T. Sherman, R.A. Lempicki, Systematic and integrative analysis of large gene lists using DAVID bioinformatics resources, Nat. Protoc. 4 (2009) 44–57, https://doi.org/10.1038/nprot.2008.211.
[45] K. Tanaka, T. Okitsu, N. Teramura, K. Iijima, O. Hayashida, H. Teramae, S. Hattori, Recombinant collagenase from Grimontia hollisae as a tissue dissociation enzyme for isolating primary cells, Sci. Rep. 10 (2020) 3927, https://doi.org/10.1038/s41598-020-60802-z.
[46] Y. Taga, M. Kusubata, K. Ogawa-Goto, S. Hattori, Highly accurate quantification of hydroxyproline-containing peptides in blood using a protease digest of stable isotope-labeled collagen, J. Agric. Food Chem. 62 (2014) 12096–12102, https://doi.org/10.1021/jf5039597.
[47] Y. Taga, M. Kusubata, K. Ogawa-Goto, S. Hattori, Stable isotope-labeled collagen: a novel and versatile tool for quantitative collagen analyses using mass spectrometry, J. Proteome Res. 13 (2014) 3671–3678, https://doi.org/10.1021/pr500213a.
[48] Y. Taga, M. Kusubata, K. Ogawa-Goto, S. Hattori, N. Funato, Collagen-derived X-Hyp–Gly-type tripeptides promote differentiation of MC3T3-E1 pre-osteoblasts, J. Funct.Foods 46 (2018) 456–462, https://doi.org/10.1016/j.jff.2018.05.017.
[49] N. Chanthra, T. Abe, M. Miyamoto, K. Sekiguchi, C. Kwon, Y. Hanazono, H. Uosaki, A novel fluorescent reporter system identifies Laminin-511/521 as potent regulators of cardiomyocyte maturation, Sci. Rep. 10 (2020) 4249, https://doi.org/10.1038/s41598-020-61163-3.
[50] S. Ricard-Blum, The collagen family, Cold Spring Harbor Perspect. Biol. 3 (2011) a004978, https://doi.org/10.1101/cshperspect.a004978.
[51] M. Yamauchi, M. Sricholpech, Lysine post-translational modifications of collagen, Essays Biochem. 52 (2012) 113–133, https://doi.org/10.1042/bse0520113.
[52] Q.A. Majid, A.T.R. Fricker, D.A. Gregory, N. Davidenko, O. Hernandez Cruz, R. J. Jabbour, T.J. Owen, P. Basnett, B. Lukasiewicz, M. Stevens, S. Best, R. Cameron, S. Sinha, S.E. Harding, I. Roy, Natural biomaterials for cardiac tissue engineering: a highly biocompatible solution, Front. Cardiovasc. Med. 7 (2020), 554597, https://doi.org/10.3389/fcvm.2020.554597.
[53] K.T. Weber, Cardiac interstitium in health and disease: the fibrillar collagen network, J. Am. Coll. Cardiol. 13 (1989) 1637–1652, https://doi.org/10.1016/0735-1097(89)90360-4.
[54] M. Pauschinger, A. Doerner, A. Remppis, R. Tannhäuser, U. Kühl, H.P. Schultheiss, Differential myocardial abundance of collagen type I and type III mRNA in dilated cardiomyopathy: effects of myocardial inflammation, Cardiovasc. Res. 37 (1998) 123–129, https://doi.org/10.1016/s0008-6363(97)00217-4.
[55] Q.-Z. Chen, S.E. Harding, N.N. Ali, A.R. Lyon, A.R. Boccaccini, Biomaterials in cardiac tissue engineering: ten years of research survey, Mater. Sci. Eng. R. 59 (2008) 1–37, https://doi.org/10.1016/j.mser.2007.08.001.
[56] R.R. de Souza, Aging of myocardial collagen, Biogerontology 3 (2002) 325–335, https://doi.org/10.1023/a:1021312027486.
[57] M.M.H. Marijianowski, C.M. van der Loos, M.F. Mohrschladt, A.E. Becker, The neonatal heart has a relatively high content of total collagen and type I collagen, a condition that may explain the less compliant state, J. Am. Coll. Cardiol. 23 (1994) 1204–1208, https://doi.org/10.1016/0735-1097(94)90612-2.
[58] M. Ieda, T. Tsuchihashi, K.N. Ivey, R.S. Ross, T.T. Hong, R.M. Shaw, D. Srivastava, Cardiac fibroblasts regulate myocardial proliferation through beta1 integrin signaling, Dev. Cell 16 (2009) 233–244, https://doi.org/10.1016/j.devcel.2008.12.007.
[59] C.M. Lapiere, B. Nusgens, G.E. Pierard, Interaction between collagen type I and type III in conditioning bundles organization, Connect. Tissue Res. 5 (1977) 21–29, https://doi.org/10.3109/03008207709152608.
[60] J. Lincoln, J.B. Florer, G.H. Deutsch, R.J. Wenstrup, K.E. Yutzey, ColVa1 and ColXIa1 are required for myocardial morphogenesis and heart valve development, Dev. Dynam. 235 (2006) 3295–3305, https://doi.org/10.1002/dvdy.20980.
[61] T. Yokota, J. McCourt, F. Ma, S. Ren, S. Li, T.H. Kim, Y.Z. Kurmangaliyev, R. Nasiri, S. Ahadian, T. Nguyen, X.H.M. Tan, Y. Zhou, R. Wu, A. Rodriguez, W. Cohn, Y. Wang, J. Whitelegge, S. Ryazantsev, A. Khademhosseini, M.A. Teitell, P. Y. Chiou, D.E. Birk, A.C. Rowat, R.H. Crosbie, M. Pellegrini, M. Seldin, A.J. Lusis, A. Deb, Type V collagen in scar tissue regulates the size of scar after heart injury, Cell 182 (3) (2020) 545, https://doi.org/10.1016/j.cell.2020.06.030, 562 e23.
[62] J. Xu, F. Xing, X. Luo, J. Gao, Y. Zhang, G. Zhang, X. Bai, C.C. Huang, Quantitation of collagen Type V in tissues by high-performance liquid chromatography coupled to mass spectrometry, Tissue Eng. C Methods 28 (2022) 95–103, https://doi.org/10.1089/ten.TEC.2022.0003.
[63] K. Uzawa, H.N. Yeowell, K. Yamamoto, Y. Mochida, H. Tanzawa, M. Yamauchi, Lysine hydroxylation of collagen in a fibroblast cell culture system, Biochem. Biophys. Res. Commun. 305 (2003) 484–487, https://doi.org/10.1016/s0006-291x(03)00799-x.
[64] D.M. Hudson, M. Garibov, D.R. Dixon, T. Popowics, D.R. Eyre, Distinct post-translational features of type I collagen are conserved in mouse and human periodontal ligament, J. Periodontal. Res. 52 (6) (2017) 1042–1049, https://doi.org/10.1111/jre.12475.
[65] Y.N. S Fujiwara, Bovine renal cortex type I collagen: high contents of 3- and 4-hydroxyprolines, J. Biochem. 89 (5) (1981) 1397–1401, https://doi.org/10.1093/oxfordjournals.jbchem.a133331.
[66] A. Rhoden, F.W. Friedrich, T. Brandt, J. Raabe, M. Schweizer, J. Meisterknecht, I. Wittig, B.M. Ulmer, B. Klampe, J. Uebeler, A. Piasecki, K. Lorenz, T. Eschenhagen, A. Hansen, F. Cuello, Sulforaphane exposure impairs contractility and mitochondrial function in three-dimensional engineered heart tissue, Redox Biol. 41 (2021), 101951, https://doi.org/10.1016/j.redox.2021.101951.
[67] A. Rhoden, T. Schulze, N. Pietsch, T.A.-O. Christ, A. Hansen, T.A.-O. Eschenhagen, Comprehensive analyses of the inotropic compound omecamtiv mecarbil in rat and human cardiac preparations, Am. J. Physiol. Heart Circ. Physiol. 322 (2022) H373–H385, https://doi.org/10.1152/ajpheart.00534.2021.
[68] S. Tohyama, K. Fukuda, Safe and effective cardiac regenerative therapy with human-induced pluripotent stem cells: how should we prepare pure cardiac myocytes? Circ. Res. 120 (2017) 1558–1560, https://doi.org/10.1161/CIRCRESAHA.116.310328.
[69] S. Tohyama, J. Fujita, C. Fujita, M. Yamaguchi, S. Kanaami, R. Ohno, K. Sakamoto, M. Kodama, J. Kurokawa, H. Kanazawa, T. Seki, Y. Kishino, M. Okada, K. Nakajima, S. Tanosaki, S. Someya, A. Hirano, S. Kawaguchi, E. Kobayashi, K. Fukuda, Efficient large-scale 2D culture system for human induced pluripotent stem cells and differentiated cardiomyocytes, Stem Cell Rep. 9 (2017) 1406–1414, https://doi.org/10.1016/j.stemcr.2017.08.025.
[70] M.T. Kozlowski, C.J. Crook, H.T. Ku, Towards organoid culture without Matrigel, Commun. Biol. 4 (2021) 1387, https://doi.org/10.1038/s42003-021-02910-8.